Mathematical modelling of glycolysis in cancer cell lines

by

Craig Amos October

Thesis presented in partial fulfilment of the requirements for the degree of Master of Science (Biochemistry) in the Faculty of Science at Stellenbosch University

Supervisor:	Prof. J.L. Snoep
Co-supervisors:	Dr. T. Kouril Dr. D.D. van Niekerk

March 2021

Declaration

By submitting this thesis electronically, I declare that the entirety of the work contained therein is my own, original work, that I am the sole author thereof (save to the extent explicitly otherwise stated), that reproduction and publication thereof by Stellenbosch University will not infringe any third party rights and that I have not previously in its entirety or in part submitted it for obtaining any qualification.

Date: 2020/12/16 .....

Abstract

Mathematical modelling of glycolysis in cancer cell lines

C.A. October

Department of Biochemistry,
University of Stellenbosch,
Private Bag X1, Matieland 7602, South Africa.

Thesis: MSc (Biochemistry)

December 2020

Most cancer cells exhibit an increase in glucose uptake and lactate production, a phenomenon known as the "Warburg effect" or aerobic glycolysis, and considered to be a hallmark of cancer metabolism.

We investigated the glycolytic flux and enzyme activities in MDA-mb-231, a highly invasive triple-negative breast cancer cell. Enzyme assays were conducted on each glycolytic enzyme to characterise the kinetic parameters required for the construction of a detailed mechanistic mathematical model. Model validation data was obtained by analysing the time dynamics of the system variables using an ion-pairing reverse liquid chromatography method for cell extract conversion of glucose to lactate. In addition, we determined glycolytic flux in MDA-mb-231 whole-cells via an extracellular flux assay, and compared it to a non-invasive cancer cell line (MCF-7).

Results showed that both cell lines generate 1.7 moles of lactate per mole of glucose consumed, though the MDA-mb-231 flux was 2-fold higher than that measured in MCF-7 cells. The initial constructed model was accurate in the prediction of the glycolytic intermediates in upper glycolysis but deviated significantly from the experimental results in lower glycolysis. We established that the model over-estimated PGM activity, as the enzyme activity is significantly lower in the experiment due to insufficient amounts of 2,3 bisphosphoglycerate (2,3-BPG) to activate the co-factor dependent PGM. We used the model to predict both conditions: with and without the addition of 2,3-BPG. The model's accuracy was satisfactory for the time-dynamics of glycolytic intermediates in both conditions, although the model predictions were far from perfect, most of the variables were constantly described, resulting in a partly validated model. Based on glucose to lactate conversion, the glycolytic behaviour in whole-cells and the cell extracts appears to be distinctly different.

Uittreksel

Wiskundige modellering van glikolise in kanker sellyne

("Mathematical modelling of glycolysis in cancer cell lines")

C.A. October

Departement Biochemie,
Universiteit van Stellenbosch,
Privaatsak X1, Matieland 7602, Suid Afrika.

Tesis: MSc (Biochemistry)

Desember 2020

Die meeste kankerselle vertoon 'n toename in glukose-opname en laktaatproduksie, 'n verskynsel wat bekend staan as die "Warburg-effek" of aërobiese glikolise, en word beskou as 'n kenmerk van kankermetabolisme.

Ons het die glikolitiese vloed- en ensiemaktiwiteite in MDA-mb-231, 'n uiters indringende drievoudige negatiewe borskankersel, ondersoek. Ensiembepalings is op elke glikolitiese ensiem uitgevoer om die kinetiese parameters te kenmerk wat benodig word vir die konstruksie van 'n gedetailleerde meganistiese wiskundige model. Modelvalideringsdata is verkry deur die tyddinamika van die stelselveranderlikes te ontleed deur gebruik te maak van 'n ioon-koppelende omgekeerde vloeistofchromatografie-metode vir die selekstrakte omskakeling van glukose na laktaat. Daarbenewens het ons glikolitiese vloed in MDA-mb-231 heel-selle bepaal deur middel van 'n ekstrasellulêre vloedtoets, en dit vergelyk met 'n nie-indringende kanker-sellyn (MCF-7).

Die resultate het getoon dat beide sellyne ongeveer 1,7 mol laktaat per mol verbruikte glukose genereer, alhoewel die MDA-mb-231-vloed tweevoudig hoër was as wat in MCF-7-selle gemeet is. Die aanvanklike gekonstrueerde model was akkuraat in die voorspelling van die glikolitiese tussenprodukte in die boonste glikolise, maar het beduidend afgewyk van die eksperimentele resultate in laer glikolise. Ons het vasgestel dat die model die PGM-aktiwiteit te hoog geskat het, aangesien die ensiemaktiwiteit in die eksperiment aansienlik laer is as gevolg van onvoldoende hoeveelhede 2,3 bis-fosfoglyceraat (2,3-BPG) om die ko-faktorafhanklike PGM te aktiveer. Ons het die model gebruik om albei toestande te voorspel: met en sonder die toevoeging van 2,3-BPG. Die akkuraatheid van die model was bevredigend vir die tyddinamika van glikolitiese tussengangers in albei toestande, alhoewel die modelvoorspellings nog

lank nie perfek was nie, is die meeste veranderlikes voortdurend beskryf, wat 'n gedeeltelik gevalideerde model tot gevolg gehad het. Op grond van glukose na laktaat-omskakeling lyk die glikolitiese gedrag in heel-selle en selekstrakte duidelik anders.

Acknowledgements

I would like to express my sincere gratitude to the following individuals and institutions:

- My supervisor Prof. Jacky L. Snoep.
- My co-supervisors Dr Theresa Kouril and Dr Dawie D. van Niekerk
- All my laboratory colleagues and Arrie Arends, our lab manager.
- My dear family and friends
- The National Research Foundation (NRF) for funding.
- The department of Biochemistry at Stellenbosch University

Contents

List of Figures

List of Tables

Abbreviations

Enzymes

AK Adenylate Kinase
HK Hexokinase
G6PDH Glucose-6-phosphate Dehydrogenase
PGI Phosphoglucoisomerase
PFK Phosphosfructokinase
ALD Aldolase
TPI Triosephosphate Isomerase
GAPDH/G3PDH Glyceraldehyde 3-phosphate Dehydrogenase
PGK Phosphoglycerate Kinase
PGM Phosphoglycerate Mutase
ENO Enolase
PK Pyruvate Kinase
LDH Lactate Dehydrogenase

Metabolites

AMP Adenosine Monophosphate
ADP Adenosine Diphosphate
ATP Adenosine Triphosphate
NAD^+ Oxidised Nicotinamide Adenine Dinucleotide
NADH Reduced Nicotinamide Adenine Dinucleotide
$NADP^+$ Oxidised Nicotinamide Adenine Dinucleotide Phosphate
NADPH Reduced Nicotinamide Adenine Dinucleotide Phosphate
GLC Glucose
G6P Glucose 6-phosphate
F6P Fructose 6-phosphate
F16BP Fructose 1,6-Bisphosphate
GAP Glyceraldehyde 3-Phosphate
DHAP Dihydroxyacetone Phosphate

B13PG 1,3-Bisphosphoglycerate
3-PG 3-Phosphoglycerate
2-PG 2-Phosphoglycerate
2,3-BPG 2,3-Bisphosphoglycerate
PEP Phosphoenolpyruvate
Pyruvate Pyruvate
LAC Lactate

Constant

K_{eq} Equilibrium Constant

Symbol

Γ Mass Action Ratio

Chapter 1

Introduction

Despite the progress made in cancer research, the disease continues to plague humanity. WHO predicts an increase in diagnosed cases, which they attribute to an ageing population and increasing risk factors, e.g. diabetes, tobacco use, etc. [1]. Since one in every six deaths can be attributed to cancer and it is regarded as a public health challenge worldwide [1]. "Cancer" is a hypernym used to categorise a multitude of diseases with various histological, bioenergetic and genetic traits, where cells undergo mutations that gives rise uncontrollable proliferation. In the body, these rapidly proliferating cells initiate tumour formation. Whereas, healthy cells adhere to a specific function that they were designated to perform, cancer cells do away with these constraints to obtain control over metabolic systems for their own needs.

Metabolic reprogramming takes place within cancer cells, leading to an alteration in nutrient acquisition and cellular bioenergetics that further improves their metabolic plasticity in a dynamic cellular environment [2]. This reprogramming is considered an essential hallmark of cancer. A frequent metabolic characteristic observed in cancer cells is an enhanced glycolytic flux, generating vast amounts of lactate, a modification referred to as the Warburg effect or aerobic glycolysis [3]. Studies have proposed that aerobic glycolysis provides a rapid supply of bioenergy independent of oxygen to sustain the unfettered proliferation of cancer cells [2, 4].

Investigations into reprogrammed metabolism observed in cancer has garnered interest since it is considered to be a potential target for cancer treatment [2, 5]. Such investigations can be greatly facilitated by computational systems biology, which can provide a holistic view of the dynamic behaviour of the metabolic network [6, 7]. This methodology involves the use of mathematical models that can elucidate the underlying controlling mechanisms and flux through the nodes within metabolic systems. Here a model of a metabolic system is constructed using mathematical expressions for its individual reactions. The expressions are parametrised by means of fitting to characterisation experiments performed on isolated system components. This method describes the bottom-up approach for model construction and is frequently utilised to

investigate the glycolytic pathway [8–10]. A well-defined and validated model can sufficiently describe a metabolic pathway within the cell and can be further used to probe the system to determine the controlling mechanism through metabolic control analysis (MCA). This analytical tool offers a means of quantifying the distribution of flux-control and sensitivity of the individual elements within the system [11]. Some studies have applied these methods to investigate cancer metabolism, though there is still a lack of detailed kinetic models of breast cancer cell lines [8, 10, 12].

In this thesis, we consider the MDA-mb-231 and MCF-7 breast cancer cell lines as our chosen model systems – with a focus on the MDA-mb-231 cell line. MDA-mb-231 is representative of highly invasive triple-negative breast cancer cells, which are hormone non-responsive [13]. This cell line has been shown to be dependent on glycolysis to generate the majority of its cellular energy (ATP) to meet its metabolic needs [14]. Patients diagnosed with triple-negative breast cancer (TNBC), have poorer therapeutic outcomes due to clinical characteristics of this basal-like subtype, which includes its invasive/metastatic properties and recurrence risk despite using chemotherapy interventions [13]. Therefore, cancer cell line representative of TNBC is a relevant model system to investigate given their limited therapeutic response and their invasive characteristics [13].

The research question of this study is: Can we explain glycolytic flux in cancer cells on the basis of its enzyme characteristics? The aim of this thesis involves constructing and validating a mathematical model of glycolysis in the chosen model system, MDA-mb-231. The broader aim of the research programme in our group is to elucidate the underlying control mechanisms of the Warburg effect in TNBC cells by using MCA and the constructed model as tool to identify possible drug targets within the glycolytic pathway. However, this is beyond the scope of this thesis. To answer the stated research question, the following objectives were defined;

- Determine the extracellular glycolytic flux of MDA-mb-231 cells and compare its flux to the non-invasive MCF-7 cancer cell line.
- Conduct *in vitro* kinetic characterisation of each glycolytic enzyme by performing enzyme assays and fitting the mechanistic rate equation to the enzyme data.
- Construct a detailed kinetic model by integrating the parametrised rate equations into ODEs – each representing the time dynamics of a metabolite in glycolysis.
- Validate the model via *in vitro* ^{14}C-labelled time-course experiment.

The following chapters documents the task undertaken to achieve the aim of this project: **Chapter 2** will elaborate on the concepts discussed in this

chapter and provide the necessary background on cancer metabolism and various mathematical modelling approaches. **Chapter 3** describes the methodology behind the experimental and computational procedures applied and their utility in this project. In **Chapter 4** we present the kinetic parameter characterisation of each enzyme in glycolysis and how we construct the mathematical model describing the change in concentration of each glycolytic metabolites. **Chapter 5** compares ion-pairing reverse liquid chromatography (IP-RPLC) analysed time-course experiments to the constructed mathematical model. Herewith, we determine whether the detailed-kinetic model is an appropriate description of *in vitro* system dynamics. The glycolytic flux of MDA-mb-231 cells were measured and was also compared to the MCF-7 breast cancer cell line to measure the difference in flux between a highly-invasive and non-invasive cancer cell line. Lastly, **Chapter 6** presents a summary of the current thesis, with a section on proposed future work.

Chapter 2

Literature Study

2.1 Introduction

According to WHO [1], cancer is globally the second leading cause of death, and cases are expected to double over the next two decades. A 2018 report by WHO estimated that 9.6 million deaths were due to cancer, with breast cancer being the most prevalent cancer affecting women worldwide [1, 15]. Studies investigating incidence, global burden and mortality rates of breast cancer, have postulated that prevalence is higher in high-income countries compared to lower- and middle-income countries, but incidences are rapidly rising in the latter [16, 17].

An estimated 12-17% of breast carcinomas are triple-negative breast cancer (TNBC) – defined by the absence of oestrogen receptor, progesterone receptor and HER2 (human epidermal growth factor receptor type 2) [13]. Evidently, endocrine therapy or HER2-targeted therapeutic approaches are not applicable to TNBC. This phenotype is biologically aggressive with a high histologic grade, which refers to its malignant and metastatic properties implying that TNBC is better able to metastasize to viscera [13].

The metabolic transformations frequently observed in cancer cells are considered to be an essential hallmark of cancer [18]. Most tumour cells exhibit alterations in metabolism, nutrient acquisition and cellular bioenergetics [4, 19]. The most common feature of metabolic dysregulation observed in tumour cells is the increased glycolytic flux under aerobic conditions, a phenomenon known as the Warburg effect or aerobic glycolysis [2, 19, 20]. Why cancer cells prefer to ferment glucose over respiration under aerobic conditions remain largely unclear. It has been suggested that the altered metabolic pathways provide the rapidly proliferating cancer cells sufficient cellular energy and intermediates for anabolic subsidiary pathways to maintain malignant properties [2, 4, 19, 21]. It was previously hypothesized that aerobic glycolysis observed in cancer cells was due to a dysfunctional oxidative phosphorylation metabolism [21, 22]. Further research established that the mitochondria remain functional and pro-

vided evidence that suggest the metabolic reprogramming is due to oncogene dysregulation (e.g. hypoxia inducible factor 1 (HIF-1), K-Ras and c-Myc), loss of tumour suppressors and up-regulation of components in the mTOR signalling pathway [5, 23, 24]. Oncogenes up-regulate glycolytic enzymes and are responsible for specific isoform expression, including the re-expression of embryonic isoforms in tumour cells, thus enhancing the flux through glycolysis in malignant cancer cells [19]. Similarly, the tricarboxylic acid (TCA) cycle is altered, whereby the pathway is partly decoupled from central carbon metabolism and intermediates, supplied by the enhanced glutaminolysis, are shunted towards the biosynthesis of macromolecules and oxidative phosphorylation (OXPHOS) [3, 24].

Numerous techniques exist to investigate the reprogrammed metabolism in cancer cells. Computational systems biology provides a method to understand the system's behaviour as a whole [6]. Systems biology is an investigative tool that can be used to obtain an in-depth understanding of biological phenomena such as a system's response to complex stimuli [6, 7]. Mathematical modelling of metabolism can be achieved by either the top-down or bottom-up approach [6]. The top-down approach, which is used in, for example, extracting information from high-throughput data ("omics" data) to construct and interpret cellular system models. Whereas, the bottom-up approach constructs a detailed model of the whole-system by characterising the individual elements that make up the system and integrating them to gain a holistic understanding of the system dynamics [6]. These mathematical models describe the time-dependent change of metabolites by employing ordinary differential equations (ODEs) [25]. This requires the parametrisation of reactions involved in the metabolic pathway that is being modelled. The Michaelis-Menten and Monod-Wyman-Changeux models are the most prevalent mechanistic models employed to describe kinetics of enzymatic reactions [26, 27]. In the bottom-up approach the equations are fitted to data from experiments performed on isolated enzymes.

Metabolic control analysis (MCA) is an analysis method to investigate control and regulation in metabolism. This approach quantitatively determines the extent of control a specific enzyme exerts on the flux of a given pathway, which can further our insight into the underlying mechanisms governing the system properties [28]. Therefore, MCA could serve as a tool to identify key reaction steps in the biological system. Differences in the metabolic networks of healthy differentiating cells and cancer cells, could point to targets for drugs that exploit this difference and potentially damage the cancer cells without harming the host tissue [29]. In this literature review, I will give a brief overview of changes that have occurred in central carbon metabolism of cancer cells, focussing on glycolysis (Section 2.2– 2.3), and modelling tools and approaches that have been used to study cancer metabolism (Section 2.4).

2.2 Glycolysis in cancer cells

The glycolytic pathway consists of a network of reactions that catabolize glucose: yielding two molecules of pyruvate, ATP and NADH from one molecule of glucose, ADP, P_i and NAD^+ [5]. Pyruvate could shunt towards the TCA cycle, and subsequently be oxidized to CO_2 with reducing equivalent oxidised via oxidative phosphorylation, a metabolic process producing up to an additional 34 molecules of ATP per molecule of glucose consumed [5]. Alternatively, glucose can also be fermented, where the pyruvate is directed to lactate production, as shown in Fig. 2.1. Fermentation maintains redox balance by regenerating NAD^+ to serve as substrate for the glycolytic pathway but sacrifices the further production of bioenergy in the form of ATP via OXPHOS. Oxidative phosphorylation, as the name suggests, requires the presence of oxygen, while fermentation can occur anaerobically. Surprisingly, tumour cells prefer the fermentation of glucose, even in the presence of adequate oxygen and functional OXPHOS [2, 3]. This phenomenon is known as the Warburg effect or aerobic glycolysis. Cancer cells exhibit an up-regulated glycolytic flux when compared to normal differentiating cells. Researchers postulated this enhanced glycolysis provides sufficient precursors for biosynthesis while meeting the energy requirements for rapid cell proliferation [2, 22]. Since aerobic glycolysis is so widely observed in cancer cells, one would expect that usage of this much less efficient pathway must provide cancer cells with an advantage over utilising OXPHOS.

2.2.1 Warburg effect

Aerobic glycolysis was discovered by Warburg and Cori in the 1920s [21]. They observed the rapid glucose consumption and high lactate production rate exhibited in tumorous cells [21, 30]. This phenomenon has been observed in various cancer types, including breast cancer [21]. Warburg postulated that aerobic glycolysis was brought about by an impaired mitochondrial function [2, 3, 22]. However, subsequent research contradicted Warburg′s theory and has shown that functioning mitochondria are required for cancer cell proliferation [2, 3]. Yet, the advantage of aerobic glycolysis over the more energy efficient OXPHOS pathway remains elusive. Studies have proposed that the metabolic reprogramming giving rise to aerobic glycolysis in cancer cells provides oxygen independent ATP production – preventing excess production of reactive oxygen species and supplying adequate intermediates for biosynthesis, whilst simultaneously generating rapid cellular energy from the increased glycolytic flux in proliferating cells [4, 19]. Aerobic glycolysis is, however, not exhibited in all tumour types or subtypes. Metabolic plasticity of some cancer cell lines allows them to switch interchangeable between fermentation and oxidative metabolism as their primary source of cellular energy [21]. Some tumorous cells display a glycolytic phenotype whereas others a more oxidative

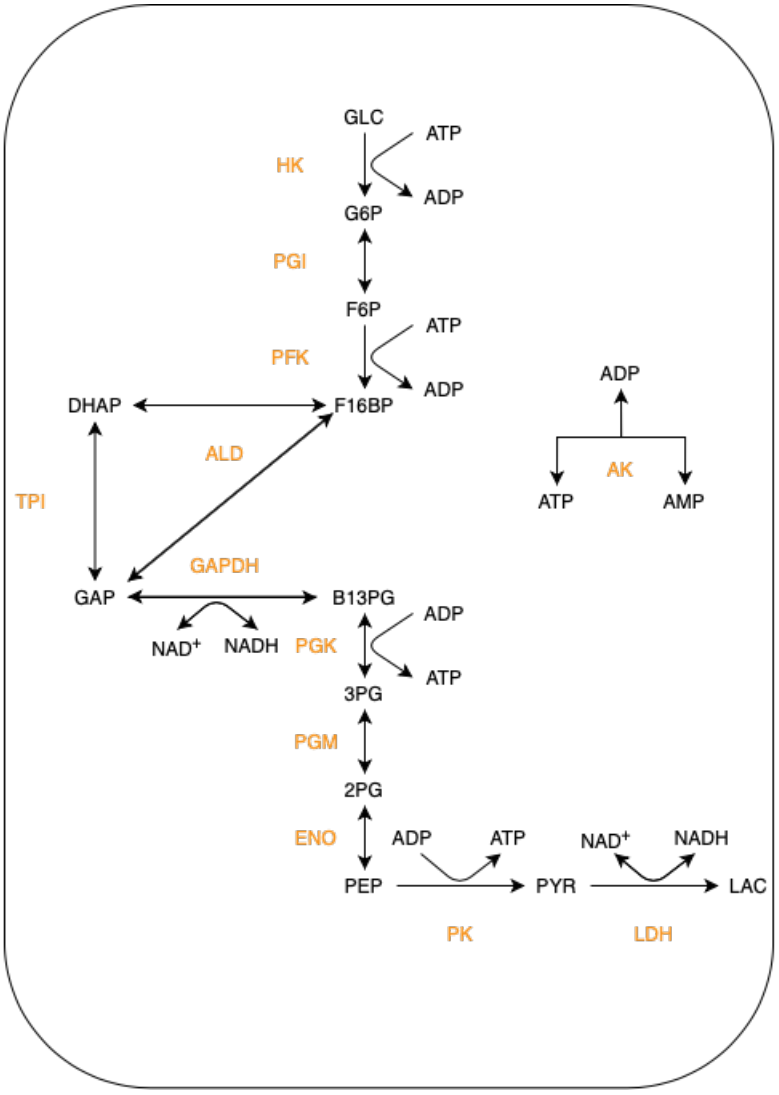

Figure 2.1: Simplified illustration the glycolytic pathway, where pyruvate directed to lactate production, as discussed in the Section 2.2. No branch pathways were shown, and the glycolytic enzymes and metabolites are displayed in orange and black, respectively.

phenotype.

Interestingly, a similar phenomenon can be observed in yeast, where it is known as the Crabtree effect [23]. Literature has drawn similarities between the Warburg effect and the Crabtree effect [31, 32]. Both exhibit similar features: an up-regulated glycolytic pathway, fermentation of glucose in the presence of oxygen and sufficient intermediate supply for rapid proliferation [31, 32].

2.3 Metabolic reprogramming

As previously mentioned, the reprogramming of metabolism can be attributed to the dysregulation of signalling pathways, oncogenes (HIF-1, K-Ras and c-Myc), and evading tumour growth suppressors [5, 24, 33]. This dysregulation leads to an increased glycolytic flux, unrestrained cell proliferation and cell growth, both elements contributing to the carcinogenic characteristics in cancer cells [4].

2.3.1 Oncogenes dysregulation

Hypoxia-Inducible Factor-1 (HIF-1) is a pleiotropic transcription factor that is involved in the adaption of normal differentiating cells under hypoxic conditions and is degraded under normoxic conditions [23, 34, 35]. It enables cells to primarily use glycolysis, an oxygen-independent pathway as a means of generating its cellular energy. The dysregulation of the HIF-1 oncogene observed in most cancer cells, operates together with c-Myc, which stimulates the up-regulation of glycolytic activity [5, 35]. This includes specific isoform expression and the re-expression of embryonic enzymes [19, 36]. The specific glycolytic enzymes that are overexpressed will be discussed in the following section.

In addition to aerobic glycolysis, metabolic transformation also enhances amino acid metabolism, and glutaminolysis is considered another key characteristic in the reprogrammed cancer metabolism [24, 36]. Glutaminolysis is a sequence of biochemical reactions that catabolize extracellular glutamine to produce glutamate and subsequently α-ketoglutarate to supply substrate to the TCA cycle [2, 3, 24]. Moreover, the oncogene, c-Myc and K-Ras are crucial regulators that contribute to the enhanced glutamine metabolism in cancer cells [24]. Therefore, oncogenes play a pivotal role in the metabolic transformation in cancer cells. The PI3K-AKT-mTOR signalling pathway coordinating with c-Myc and the loss of tumour suppressors (e.g. p53) are also significant factors involved in cancer metabolism, but are beyond the scope of this review [5, 24, 33].

2.3.2 Up-regulation and specific isoform expression of glycolytic enzymes

As previously stated, the metabolic reprogramming in cancer cells is induced by the dysregulation of oncogenes, signalling pathways and tumour suppressors. The reprogramming in cancer cells frequently results in the upregulation of glycolytic flux [5, 23, 24]. This is achieved by alterations in the isoform expression pattern of glycolytic enzymes and the overexpression of these enzymes in cancer cells when compared to the normal differentiating cells [37]. The following subsections, present a description of the modifications and up-regulation of key glycolytic enzymes contributing to the transformed metabolic behaviour and enhanced glycolytic flux in cancer cells. It should, however, be noted that the effects induced by specific glycolytic enzymes discussed below, are not integrated and it is therefore speculative to attribute systemic changes, such as flux increase to specific enzymes at this point.

2.3.2.1 Hexokinase

Hexokinase (HK) is responsible for the conversion of glucose to glucose-6 phosphate: This is the first committed step in glycolysis, which captures glucose within the cell. HK is a key enzyme in glycolysis as it has been shown to exert considerable control over the glycolytic flux [37]. Mammalian cells encode four isoforms of HK (HK-I, -II, -III and glucokinase). Their expression is tissue-specific and they exhibit distinct kinetic properties. Oncogene, HIF-1α, targets the expression of HK-I and transactivates HK-II by interacting with c-Myc in cancer cells [37, 38]. In cancer cells the more prevalent isoform overexpressed is the HK-II, whereas in normal differentiating cells, this HK-II isoform is primarily expressed in heart, adipose, skeletal muscle and embryonic tissue [33, 37]. Studies suggest the purpose of overexpression of HK-II is due to the genome accessibility of the HK-II locus for transcriptional reprogramming [33].

A unique feature of HK-I and HK-II is their association with the mitochondria. Literature has demonstrated that a phosphorylated HK-I or HK-II can attach to the voltage-dependent anion channel (VDAC) located on the outer membrane of mitochondria [23, 38]. The binding of HK to mitochondria confers two potential metabolic advantages: Firstly, it provides HK with mitochondrial generated ATP for more efficient glucose phosphorylation. This enables HK-I and HK-II to be less sensitive to G6P product inhibition [37]. Secondly, it prevents the proapoptotic protein, Bax from binding to the VDAC1 and thus inhibits the cytochrome c (Cyt c) initiated cell apoptosis [23, 38]. Therefore, up-regulation of HK-I and HK-II isoforms contributes to the enhanced glycolytic flux but also the malignant properties of cancer cells, due to HK inhibiting Bax-induced cell death.

2.3.2.2 Phosphofructokinase

Phosphofructokinase (PFK) catalyses the second committed step in the glycolytic pathway, phosphorylating fructose 6-phosphate (F6P) to fructose 1,6-bisphosphate (F16BP) by transfer of phosphate from ATP. PFK is highly regulated and considered to be a pivotal enzyme in glycolysis as it is often a major flux-controlling step [12, 22]. PFK is allosterically regulated by ATP, and citrate acts an a negative-feedback inhibitor, whereas fructose 2,6-bisphosphate (F2,6BP) and AMP acts as activators [39, 40]. This tetrameric enzyme is encoded by three different genes in mammalian cells, which express PFK in either a homo- or hetero-tetramer and, depending on the subunits, as the L, M or C isoform [40]. Isoforms expressed are also tissue-specific with PFK-L and C isoforms predominantly expressed in liver and placenta tissue [37, 40]. The PFK-M isoform is primarily located in skeletal muscle tissue, whereas in other tissues PFK-M is normally expressed as part of a mixture of PFK isoforms. Similar to hexokinase, the various PFK isoforms exhibit different kinetic properties. For example, the PFK-L is the least sensitive to citrate inhibition, and PFK-M has the highest affinity for F6P. Furthermore, PFK-M has a higher resistance to ATP substrate inhibition in comparison to PFK-C. In the context of oncogene dysregulation in cancer cells studies have stated that HIF-1α targets the up-regulation of the PFK-L isoform, although the PFK isoform expression may differ across cancer cell types [40]. The MDA-mb-231 breast cancer cells favour the up-regulation of the PFK-L isoform, whereas the HeLa cells predominantly overexpress the PFK-C isoform [40, 41]. Although, the reason for expression of a specific isoform in cancer cells is unclear, the overexpression of PFK facilitates an increase in glycolytic flux.

Additionally, mammalian cells express phosphofructokinase-2 or 6-phosphofructo-2-kinase/fructose-2,6-bisphosphatases (PFKFBs) that are responsible for generating F2,6BP from F6P [22]. F2,6BP is a potent allosteric activator of PFK-1 as this metabolite relieves inhibitory effects of ATP and citrate [42]. PFKFB is encoded from four genes and its expression is also tissue-specific leading to six isoforms with the oncogene-facilitated overexpression of PFKFB3 being most prevalent in cancer cells, such as breast and lung cancers [5, 42]. The flux-control of PFK and the PFKFB generated F2,6BP, further favours an increased glycolytic flux. Interestingly, a recent study has shown that the PFKFB4 (6-phosphofructo-2-kinase/fructose-2,6-bisphosphatase 4) isoform is bifunctional and also acts as a protein kinase, phosphorylating the SRC-3 (oncogenic steroid receptor co-activator-3) protein. A phosphorylated SRC-3 has been shown to stimulate the increase in transcriptional activity to sustain malignant properties and tumour metastasis in breast cancer cells [43].

2.3.2.3 Phosphoglycerate Mutase

Phosphoglycerate mutase (PGM) catalyses the reversible conversion of 3-phosphoglycerate (3-PG) to 2-phosphoglycerate (2-PG). PGM is a dimeric enzyme with two isoforms, PGM1 and PGM2, found in mammalian cells, with the PGM1 up-regulated in several cancers [37, 44]. Both isoforms require 2,3-bisphosphoglycerate as co-factor [37]. In addition, PGM is capable of converting PEP to pyruvate at high PEP concentrations [33]. The reaction is apparently achieved by transferring the phosphate from PEP to a histidine group located in the active site of PGM [39]. PGM is not a flux-controlling step, however, it has been shown to facilitate and modulate flux over anabolic pathways branching from glycolysis, such as the serine synthesis and pentose phosphate pathways (PPP) [39]. The latter metabolic pathway can be inhibited by 3-PG, whereas it serves as substrate for the serine synthesis pathway. PGM plays a role in the control of glycolytic branches into biosynthetic pathways and is therefore key in sustaining tumour cell proliferation and growth [39].

2.3.2.4 Pyruvate Kinase

Pyruvate kinase (PK) catalyses the last committed dephosphorylation reaction in glycolysis by transferring the phosphate from PEP to ADP, yielding pyruvate and ATP. In mammalian cells there are two isoforms of PK: PKM1 which is prevalent in skeletal muscle, heart and brain tissue, and PKM2 predominantly expressed in embryonic stems cells and leukocytes, of the two isoforms, the PKM2 is targeted by HIF-1α for overexpression in tumour cells [37, 45, 46]. The difference in kinetic properties between in M1 and M2 isoforms are: M1 is active constitutively whereas M2 is subject to extensive regulation by phosphorylation, the enzyme′s conformational state (tetrameric or dimeric) and allosteric activation by serine and the upstream metabolite, fructose 1,6-bisphosphate (F16BP) [33, 46]. Moreover, the dimerization of PKM2 is induced by protein interactions with tyrosine-phosphorylated-protein peptides and oncoproteins, changing the conformation from highly active tetrameric enzyme to a less efficient dimeric state [37, 46]. This triggers the release of allosteric activators and thus reduces PKM2 activity. The PKM2 isoform with reduced enzyme activity is frequently observed in cancer cells [37].

Literature describes that tumour cells express the M2 isoform to regulate the relationship between glycolysis and providing precursors for anabolic subsidiary pathways, such as the serine pathway [47]. A high concentration of serine serves as an PKM2 activator, channelling more pyruvate to lactate dehydrogenase (LDH). However, under low serine concentration the PKM2 activity decreases and this results in the accumulation of glycolytic intermediates for anabolic pathways [39, 47]. Xie *et al.* [48] implied that a key function of PKM2 as well as of LDH is to rapidly drive upstream glycolytic intermediates through to lactate. Irrespective of the inhibitory effects causing conformational

changes, PKM2 activity within tumour cells still exceeds that of the glycolytic flux [48]. Despite the role that PKM2 plays in glycolysis, the enzyme is not a 'rate-limiting step' nor does it have significant control over the glycolytic flux in cancer cells [12, 37].

2.3.2.5 Other glycolytic enzymes

In the subsections above we addressed the key glycolytic enzymes and are targeted for up-regulation and either exert significant flux-control or fulfil a unique role in cancer metabolism. The expression of numerious other glycolytic enzymes is elevated by oncogenes. The oncogenes, namely HIF-1α, c-Myc and K-Ras are known to up-regulate the expression of various glycolytic enzymes [49, 50]. Some glycolytic enzymes have multifaceted roles, which could be the reason for their overexpression. The up-regulation of PGI, PGK and ENO-α are such examples, as they contribute to the cell proliferation and metastatic properties. The aldolase A isoform and TPI is frequently overexpressed in cancer cells. Overexpression of TPI has been postulated to prevent methylglyoxal production from DHAP accumulation that might occur from the enhanced glycolytic flux, given that methylglyoxal has anti-cancer features [49]. GAPDH and the LDH-A isoform are also up-regulated in cancer cells [51]. These two enzymes serve a multitude of functions, where a phosphorylated LDH-A along with GAPDH facilitates destabilization of DNA-double helix and together functions as a transcription factor [51]. The LDH-A isoform consists of four M subunits and is usually up-regulated in cancer cells by HIF-1/2α , c-Myc and K-ras. Further, the LDH-A isoform possesses the highest affinity for pyruvate [49, 50]. Taken together, the up-regulation of these enzymes could potentially contribute to the enhanced glycolytic flux in cancer cells, despite their apparent low flux control.

2.3.2.6 Transporters associated with glycolysis

Some metabolite transporters play a pivotal role in glycolysis and are up-regulated in concurrence with the glycolytic enzymes in most cancer cells. This subsection will briefly discuss the role of transporters although it is not the focus of this study. The glucose transporters (GLUTs) and monocarboxylic transporters (MCTs) are the most notable transporters up-regulated in the enhanced glycolysis of cancer cells. GLUTs modulate the influx of glucose and other sugars across the plasma membrane into the cell. Numerous isoforms are expressed in mammalian cells but only four GLUT isoforms (GLUT1 – 4) favour the transport of glucose [37]. Similarly to the intra-cellular enzymes, the specific isoform expression pattern of transporters is tissue-specific. Expression of GLUT1 and 3 isoforms is targeted by HIF-1α for overexpression and insulin-sensitive GLUT4 isoform is downregulated in tumour cells [37]. Hence, the GLUT expression pattern in cancer leads to an increased influx of glucose for

the enhanced glycolytic pathway that is also largely independent of insulin stimulation [37, 52].

MCTs are also important to maintain glycolytic flux. There are 4 isoforms MTCs (MCT1 – 4) responsible for the H^+ coupled efflux of lactate. The MCTs are symport transporters, and the direction of transport is dependent on the gradient of protons and monocarboxylate. Regardless, most cancer cells generate large amounts of lactate, which generally results in the efflux of lactate. The oncogene HIF-1α triggers the overexpression of MCT4 and c-Myc the overexpression of MCT-1 in cancer cells. Inhibition of both MCT1/4 was demonstrated to obstruct cell growth as lactate build-up resulted in a cytostatic effect, whereas, the up-regulation of MCT4 has been demonstrated to significantly increase glycolytic flux [12, 36]. Research has established that glucose import and lactate export exert a substantial control over the glycolytic flux [12]. Therefore, overexpression of GLUT1/3 and MCT1/4 are key elements in aerobic glycolysis.

2.3.3 Glutaminolysis

Glutamine is the second most important growth-supporting carbon source after glucose, and glutamine is required to sustain rapid cell proliferation as the absence of glutamine has shown to result in cell arrest [2, 53]. Rapidly proliferating cancer cells show an elevated glutamine influx rates and sometimes become dependent on glutamine, known as glutamine addiction, however, this characteristic is not universal [54]. An increase in glutaminolysis flux is stimulated by c-Myc upregulation, and K-Ras has been shown to be responsible for the decoupling of the glycolysis and glutamine metabolism [24, 50, 54]. The up-regulation of glutamine transporters, glutaminase and glutamate dehydrogenase attribute to high glutamine influx.

Glutaminolysis provides the necessary carbon molecules in the form of α-ketoglutarate for TCA anaplerosis. The glutamine-derived carbon is either designated to generate aspartate for anabolic subsidiary pathways or OXPHOS [49]. However, in cases where glutamine is consumed in excess, alanine and lactate production is favoured instead of complete oxidation. The glutamine-derived nitrogen is assimilated into biosynthetic pathway, e.g. nucleotide and amino acid production, and when there is a surplus of glutamine-derived nitrogen, it is secreted as alanine and ammonia [55]. DeBeraridinis *et al.* [55] postulated that the glutamine metabolism is to conserve TCA and mitochondrial activity in c-Myc reprogrammed cells by supplying glutamine-derived oxaloacetate. Glutamine therefore functions as a carbon source for anaplerotic precursors, provides nitrogen source for biosynthesis, function as an additional free energy source and is a requirement for growth and rapid proliferation of cancer cells [55]. Glutaminolysis will, however, not be explored further in this project.

2.4 Mathematical modelling of metabolism

As is clear from the previous section, many changes in enzyme kinetic parameters can occur in cancer cells and to integrate the effects of these changes, mathematical models can play an important role. There are different modelling approaches in systems biology, e.g. top-down and bottom up approaches and the mathematical models that describe metabolism can differ in complexity, scale and level of detail [6]. In the current study, we applied the bottom-up approach to investigate metabolism.

The kinetics of each enzyme catalysed reaction in the pathway is characterised by fitting mechanistic rate equations to the data from isolated enzyme kinetic assays. The best-known mathematical description of enzyme kinetics is the Michaelis-Menten rate equation:

$$v = \frac{V_{max} \cdot S}{K_m + S} \tag{2.1}$$

Here v is the rate at which the enzyme converts substrate to product and $\mathrm{V_{max}}$, is the maximal specific activity, S the substrate concentration and $\mathrm{K_m}$ is known as the Michaelis constant. The $\mathrm{K_m}$ equals the substrate concentration at $\frac{1}{2}$ $\mathrm{V_{max}}$. The Michaelis-Menten description of reactions can be expanded to include reversible multi-substrate and product reactions with inhibitors. However, this description cannot be used for enzymes with cooperative binding kinetics. The Monod-Wyman-Changeux (MWC) transition model is suitable to describe the kinetics of cooperative enzymes, such as PFK and PK. Marzen *et al.* [26] provide further background on MWC models and their application in biological systems.

Classic enzyme kinetic characteristic experiment can be used to parametrise the rate equation. These experiments typically involve determining initial rate kinetics by providing substrate and/or product to an enzyme and measuring the reaction rate by directly or indirectly measuring the rate of appearance of a product or disappearance of a substrate. To obtain a consistent and realistic model these experiments must be performed under conditions that mimic the cytosolic environment [9]. The parametrised rate equation form the basis for the construction of a well-defined system of ODEs representing each metabolite in the system and whose integration yields the concentration of metabolites as a function of time [56]. ODE-based mathematical models are widely used for biological systems, e.g. glycolytic models of yeasts and various mammalian cell models [8, 9, 50]. Typically, ODE-based metabolic models are validated using independent experiments of intermediate metabolite concentrations in the complete intact system and comparing this to model predictions.

High-throughput data or ′omics′ information can also be used to validate detailed kinetic models. Metabolomics provides large-scale data similar to other ′-omics′ but involves the identification and quantification of metabolites present within a cell/organism. An array of strategies can be implemented to procure metabolome data, e.g. metabolic profiling. The quantification of metabolites is primarily determined using spectroscopic and separation-based-techniques, which is often coupled to a mass spectrometer. A more reliable approach, is the tracer-based metabolomics, which, as the name suggests, utilises stable isotopes such as ^{13}C-labelled substrate to trace the flux within a biological system. By converting the metabolomic data to fluxomic data the flux of metabolites through the system can be determined. One can describe metabolomics as capturing a moment of all the present metabolites at a given time, whereas fluxomics captures the dynamics of metabolism in a time-dependent fashion. Although these strategies have limitations, they are suitable for analysis of the glycolytic pathway. Flux dynamics based on metabolomics can be useful for the validation of mathematical models or their construction (as is the case with mesoscale models). In the present study, integrated metabolomic data is used to validate the detailed kinetic model that is constructed.

Once a model has been constructed and validated, metabolic control analysis (MCA) can be used to quantify the control that an individual element has on variables in the metabolic network [28]. Classic MCA requires the model to simulate an open system, which is achieved by clamping particular variables leading to constant reaction rates and steady-state metabolite concentrations, for further background refer to [11, 28]. MCA refutes the notion of a ″rate-limiting step″, implying that altering a single step would change the flux of the pathway equivalently and adjusting the activity of other enzymes would have no effect on the system [8]. Although, this phenomenon does sometimes occur, in most cases flux-control is distributed across various enzymes in the pathway but not necessarily equally distributed.

MCA defines three types of coefficients; control coefficient, elasticity coefficient and response coefficient. The flux control coefficient is defined as the effect that a fractional change in the rate of an enzyme, v, has on the flux of the pathway, J, or the steady-state concentration of a metabolite, S. This can be defined as either change in flux or metabolite concentration, but for the purpose of simplicity only the former will be used here:

$$C_v^J = \frac{d\ln J}{d\ln v} \tag{2.2}$$

The degree to which an effector or parameter, p can alter the enzyme rate, v in the system is known as the elasticity coefficient and is mathematically expressed as:

$$\varepsilon_p^v = \frac{\partial\ln v}{\partial\ln p} \tag{2.3}$$

Lastly, the response coefficient, which combines the flux-control and elasticity coefficients, is defined as the fractional change in the steady-state of the system as a result of fractional change in an effector or parameter, p. The response coefficient is mathematically expressed as:

$$R_p^J = \frac{d \ln J}{d \ln p} = C_v^J \cdot \varepsilon_p^v \tag{2.4}$$

Among the coefficients discussed, the control coefficient is the most applicable to this thesis and the model examples presented in the subsection that follows. A control coefficient can determine the magnitude to which the perturbation of an enzymatic step will change the steady-state of the system. Hence, using MCA, researchers can identify the major flux-controlling reaction(s) within a metabolic network. Accordingly, the application of MCA has garnered interest as a tool for the development of drug therapies for cancer treatment, the rational being that these drugs activate or inhibit an enzyme that has a large control over the flux in disease associated pathways .

2.4.1 Modelling glycolysis in cancer cells

Marin-Hernandez *et al.* [8] constructed mathematical models based on detailed kinetic information, but also fluxomics data to investigate aerobic glycolysis in HeLa cervix cells and AS-30D rat hepatoma cells. The kinetic data was obtained experimentally from coupled enzyme assays conducted on the cell extract of the two cell lines, and subsequently parametrised enzyme kinetic rate equations based on Michaelis-Menten mechanisms and employed the MWC transition model where applicable (PFK and PK). They also studied enzymes activities in ancillary pathways, e.g. transaldolase, transketolase and glucose 6-phosphate dehydrogenase in the pentose phosphate pathway (PPP). ODEs were applied to solve for the glycolytic intermediate concentration as a function of time. The model simulated the steady-state of glycolysis at physiological glucose and hypoglycaemic conditions in AS-30D, and the HeLa cell line under hypoxic and normoxic conditions. In addition, the researchers determined the flux control distribution across the various enzymes in the pathway via MCA under the different conditions. They simulated intermediate steady-state concentrations and validated the simulated results, by using the control distribution results obtained via elasticity analysis as their reference parameters. The same group further investigated the effect that an alteration in isoenzyme expression pattern under various glycaemic conditions (2.5, 5 and 10 mM glucose) has on the flux distribution among glycolytic enzymes [57]. Similar to their previous work, they examined steady-states and flux-control among the various enzymes in the HeLa cell line and to a limited extent in MCF-7 breast cancer cells. Both studies used MCA to determine control coefficients by simulating and conducting enzyme titration experiments to identify

which enzymes may reduce flux in glycolysis and serve as potential drug targets. Interestingly, they found that the expression pattern changes under the various glucose conditions, which in turn slightly changed the flux-control distribution [8, 57]. Similarly, Shestov *et al.* [10] constructed a detailed kinetic cancer cell model, performed perturbation experiments, MCA and integrated the model with metabolomic data. They found that at a high F16BP concentration, GAPDH is the step in aerobic glycolysis with the most control. Interestingly, this would imply that GAPDH could serve as a target to limit the flux through aerobic glycolysis.

In addition to the detailed kinetic models, a mathematical model was constructed that incorporates omics (fluxomics and transcriptomics) to simulate the oncogenic K-Ras induced decoupling of the glucose and glutamine metabolism in the K-Ras transformed NIH3T3-derived cell line [50]. Authors of the study used ^{13}C-metabolic flux analysis and non-targeted tracer fate detection, including transcription information to study how K-Ras may govern the up-regulation and decoupling of glycolysis from oxidative TCA. Tanner *et al.* [12], by using metabolomics data and MCA, identified that glucose import and phosphorylation, F16BP production and lactate export exert the largest flux-control on glycolysis and that no lower glycolytic enzymes do. To do this they systematically overexpressed each glycolytic enzyme and measured the extent to which glycolytic flux affected. There are numerous other examples of detailed kinetic models and mesoscale models found in the literature [9, 56, 58–60].

2.4.1.1 Targeting metabolism for cancer therapy

Inhibiting metabolic pathways, particularly central carbon metabolism (glycolysis), as a feasible anti-cancer strategy, requires certain conditions to be fulfilled. The potential drug should be detrimental to the intended tissue with minimal effects in healthy cells. Tumour cells are similar to the normal tissue from which they originated. This presents a potential obstacle as the similarity in enzymes, could lead to toxicity of a drug in healthy cells. Hence, targeting metabolism as an anti-cancer approach depends on whether normal proliferating cells subjected to inhibition of a specific step in the pathway would be negatively affected.

Numerous drugs already exist that target transporters and enzymes in glycolysis. An example is 2-Deoxyglucose (a competitive inhibitor) targeting GLUTs and HK-II, which plays a pivotal role in the aerobic metabolism of cancer cells [2, 61]. But glycolysis is a central pathway in all cells and the dose required to inhibit flux in cancer cells could also be damaging to host tissues. Additionally, a drug used in diabetes treatment, metforming (an AMPK activator), inhibits mitochondrial complex 1 in OXPHOS thereby preventing ATP production. This results in cell death when glucose availability is inadequate to sustain glycolysis. This drug is currently undergoing clinical trails for

cancer treatment [2]. Evidence suggests targeting aerobic glycolysis in cancer requires multiple drug targets for the drug to be effective. Interestingly, it has been documented that OXPHOS is up-regulated when glycolysis is inhibited, therefore the metabolic plasticity of cancer cells is a noteworthy obstacle to overcome for metabolism to be a viable option for cancer treatment. However, this also highlights the investigative tools that can be utilized to identify potential drug targets [5].

Systems biology strategies are appropriate tools to analyse cancer metabolism, which would provide the necessary interpretation of the metabolic behaviour to detect vulnerabilities in the system [2]. As stated previously, MCA quantitatively describes the degree of control each enzyme exerts on the pathway flux. If control mechanisms in normal proliferating cells differ from those in malignant tumour cells, it presents an opportunity to employ a network-based selective drug that exploits the vulnerabilities in cancer metabolism without damaging the host [29]. This principle of differential control analysis has been demonstrated *in vitro* with a co-culture of *Tropanosoma brucei* parasites and erythrocytes [29]. The variation in flux-control distribution between *T. brucei* and erythrocytes was sufficient for selective network-based targets. Inhibiting GAPDH and GLUTs significantly reduced the glycolytic flux of *T. brucei* without being toxic to the erythrocyte metabolism [29]. By extension, this approach could be applied for the treatment of cancer, to develop new drugs or re-purpose existing drugs for network-based selectively to target cancer while minimising damage to host tissues.

2.5 Summary

In Chapter 2 we reviewed mechanisms that contribute to the enhanced glycolytic pathway observed in cancer cells and mathematical models employed to investigate cancer metabolism. We also highlighted the potential impact that the up-regulation of glycolytic enzyme and isoform expression patterns may have on glycolysis.

Following this, we discussed studies utilising models to describe metabolism in cancer, where experimental data, and mathematical models and tools were combined to simulate and probe the dynamic behaviour of metabolism. In conclusion, using mathematical tools to investigate cancer metabolism could give further insight into its dynamic behaviour and potentially serve as a tool to develop sensible drug therapies for cancer treatment. Specifically, the differential control analysis method applied in [29] to distinguish between cancer cells and normal cells based on MCA seems promising.

Chapter 3

Methodologies

3.1 Tissue culture and harvesting protocol

MDA-mb-231 freezer stocks were kindly provided by Prof. Donita Africander (Stellenbosch University), and the MCF-7 cell line was donated by Karen van Eunen (Faculty of Medical Sciences at the University of Groningen). MDA-mb-231 and MCF-7 human breast adenocarcinoma cells lines were cultured in low-glucose DMEM (*ThermoFisher*) (1 mg/mL) growth media, supplemented with 10% v/v fetal bovine serum (FBS) (*Gibco*), 2 mM L-glutamine (*Sigma-Aldrich*) and 2% v/v 100 mg/L glucose solution (*Gibco*), but no PenStrap was added. Cells were incubated at 37°C in a humidified atmosphere (5% CO_2) as stationary monolayer cultures. The MDA-mb-231 and MCF-7 cell lines were screened for mycoplasma infection. Both cell lines tested negative.

Cells were grown until 80 – 100% confluence was achieved before cells were harvested. A trypsinisation method was employed to harvest cells in an attempt to keep cells intact. In this protocol cells were detached from the culture surface after ± 5 min via 10% v/v Trypsin-EDTA (*Sigma-Aldrich*) in PBS solution (*Sigma-Aldrich*). Subsequently, cells were centrifuged at 60 relative centrifugal force (RCF) for 3 mins at 4°C, then resuspended in DMEM to inactivate the trypsin, followed by another centrifugation step. Supernatant was removed and cells were resuspended in 50 mM Tris/HCL (pH 7.0) and centrifuged (at 60 RCF for 3 mins at 4°C), this wash step was performed twice. Upon completion, the pellet was resuspended in Tris/HCL (pH 7.0) supplemented with 1 mM PMSF (Phenylmethylsulfonyl Fluoride) (*Sigma-Aldrich*) and 1 mM DTT (Dithiothreitol) (*Sigma-Aldrich*) and stored in -80 °C. The harvesting protocol for the ^{14}C-labelled time-course experiment will be highlighted in Section 3.7. All the experiments were performed within the first 3 – to – 5 passages after thawing the MCF-7 and MDA-mb-231 cell lines. The total passage for the MDA-mb-231 and MCF-7 cell line did not exceed 77 and 12, respectively.

3.2 Lysate Preparation

Cytosolic extracts were prepared to perform enzyme assays. The cell lysate was obtained by adding Triton X-100 (*Unitek*) to the whole-cells harvested (at a final concentration of 0.1 % v/v Triton X-100). Cells were centrifuged at 20 817 RCF for 15 minutes at 4°C. The collected supernatant contains the enzymes required to perform assays and these cell extracts were either immediately used for experiments or briefly stored on ice (no longer than 4 h) before conducting experiments.

3.3 Bradford Protein Determination

Bradford protein determination was conducted to measure the protein concentration in each MDA-mb-231 and MCF-7 cell extract to normalise experimental data [62]. For this assay a standard linear range (0.007 – 1.0 mg/mL) was generated by using Bovine Serum Albumin (BSA) (*Sigma-Aldrich*). The cell lysates were diluted with MilliQ H_20 to fall within this range and absorbance was measured at 450 nm and 595 nm spectrophotometrically.

3.4 Enzyme Characterisation

3.4.1 Coupled-enzyme assays

All glycolytic enzyme activities were characterised *in vitro*, i.e. performed on cytosolic extract to determine maximal specific activity and rate constants for each substrate, product and co-factor. These enzyme activity determination protocols were adapted from Teusink *et al.* [9]. The forward and reverse reactions were performed in assay buffer (0.1 M Tris pH 7.0, 15 mM NaCl, 0.14 mM KCl, 0.5 mM $CaCl_2$, supplemented with 5 mM Phosphate Buffer pH 7.0) at 37°C by measuring the $NAD(P)^+$ reduction or NADH oxidation at 340 nm in a spectrophotometer(*BMG LABTECH SPECTRstar^{Nano}*) using 96-well microtiter plates(*Greiner*). The spectrophotometer measures the change in absorbance over time (Δ A/min at 340 nm). However, enzyme catalytic activity is expressed as U that is defined as the unit of enzyme required to catalyse the conversion of 1 μmol substrate per min (μmol/min). Therefore, the absorbance data was converted from ΔA/min to μmol/min by using the Beer Lambert law, $A = \varepsilon cl$. From this equation a rate can be determined using Eq. 3.1: Here, T_{vol} is the total volume in the assay well, (ε) the extinction coefficient of NADH (6.22 $cm^{-1}.mM^{-1}$), ℓ is the optical path length and the T_{prot} protein concentration of the cell extract determined via the Bradford protein determination assay. To therefore obtain the enzyme specific activity

(U/mg).

$$rate = \frac{c}{min} = \frac{(\Delta A/min) \cdot T_{vol}}{T_{prot} \cdot \varepsilon_{NADH,340nm} \cdot \ell} \tag{3.1}$$

Not all reactions directly consume or product NAD(P)H. In such a case the enzyme of interest is coupled via a common intermediate to one or more enzymes that lead to NAD(P)H production or consumption. For this study we employed coupled enzymes that had a final concentration of 5 U/mL. All reactions were determined under initial-rate conditions (i.e. the concentrations of substrate and products remain sufficiently constant by experimental design) and pre-heated to 37°C before initiating with substrate or co-factor. The total volume in each well was 100 μL for all enzyme characterisation experiments. For the controls, the varying component was not added to the microtiter plate well and for characterisation of bi-substrate enzymes, one substrate remained at a fixed concentration whilst the other was being varied and vice-versa. Furthermore, magnesium was added to the reaction mixture whenever adenosine phosphates were used in the assay. The concentration of Mg^{2+} was kept 2-fold greater than the adenosine phosphate concentration used. All the enzymes and reagents used in the characterisation (flux and validation) experiments were obtained from *Sigma-Aldrich* unless stated otherwise.

For reference, the following enzymes and metabolites abbreviations are defined: AK, adenylate kinase; ALD, aldolase; ENO, enolase; GAPDH/G3PDH, glyceraldehyde 3-phosphate dehydrogenase; HK, hexokinase; G6PDH, glucose-6-phosphate dehydrogenase; LDH, lactate dehydrogenase; PFK, phosphofructokinase; PGI, phosphoglucoisomerase; PGK, phosphoglycerate kinase; PGM, phosphoglycerate mutase; PK, pyruvate kinase; TPI, triosephosphate isomerase; GLC, glucose; G6P, glucose 6-phosphate; F6P, fructose 6-phosphate; F16BP, fructose 1,6-bisphosphate; GAP, glyceraldehyde 3-phosphate; DHAP, dihydroxyacetone phosphate; B13PG, bis 1,3-phosphoglycerate; 3-PG, 3-phosphoglycerate; 2-PG, 2-phosphoglycerate; PEP, phosphoenolpyruvate; PYR, pyruvate; LAC, lactate; 2,3-BPG, 2,3-bisphosphoglycerate.

Adenylate Kinase: The forward reaction was characterised by conversion of ADP (0 – 20 mM) to ATP and AMP, and coupling the reaction to hexokinase and G6DPH in the presence of GLC (2.5 mM) and $NADP^+$ (1 mM). The reverse reaction of adenylate kinase is a bi-substrate reaction therefore one substrate was kept fixed at saturating concentrations while varying the concentration of the other. To achieve characterisation of the reverse reaction the ATP (0 – 10 mM) and AMP (0 – 10 mM) conversion to ADP was linked to PK and LDH in the presence excess of NADH (1 mM) and PEP (1 mM).

Hexokinase: The phosphorylation reaction converting GLC (0 – 10 mM) to G6P by utilising ATP (0 – 7.5 mM) was assayed by coupling the reaction to G6PDH in the presence of $NADP^+$ (1 mM), allowing for its reduction via

G6PDH. Furthermore, ADP (0 – 20 mM) and AMP (0 – 20 mM) inhibition was also characterised by varying inhibitor concentration while substrates concentrations remained fixed.

Phosphoglucoisomerase: The forward reaction was assayed by coupling the reaction to PFK, ALD, TPI and G3PDH, including the required co-factors ATP (4 mM) and NADH (1 mM). The reaction was initialised with G6P (0 – 35 mM). The reverse reaction converted F6P (0 – 32 mM) to G6P, which was coupled to G6PDH, allowing for the reduction of $NADP^+$ (1 mM).

Phosphofructokinase: Characterisation of this phosphorylation reaction was performed by varying concentrations of F6P (0 – 30mM) or ATP (0 – 10 mM). This reaction was coupled to TPI, ALD and G3PDH, whereby NADH was oxidised. In addition, PFK inhibition by AMP (0 – 8 mM) and ADP (0 – 5 mM) was also determined under constant concentrations of F6P (10 mM).

Aldolase: The forward reaction splitting F16BP (0 – 10 mM) to DHAP and GAP was assayed coupling the reaction to TPI, G3PDH and provided the required co-factor, NADH (1 mM) for the indicator reaction.

Triosephosphate Isomerase: Characterisation of this enzyme catalysed reaction was performed in only the reverse direction, GAP (0 – 10 mM) to DHAP and linked to G3PDH in the presence of NADH (1 mM).

Glyceraldehyde 3-Phosphate Dehydrogenase: This reaction was assayed in the reverse direction facilitated by coupling the reaction to PGK and initialised with 3-PG (0 – 60 mM) and ATP (4 mM) leading to 1,3-BPG formation. This allowed for the conversion of 1,3-BPG to GAP by oxidation of NADH (0 – 1 mM).

Phosphosglycerate Kinase: Characterisation of the reverse direction was performed via coupling the enzyme to GAPDH, to determine PGK′s kinetics for ATP (0 – 10 mM) and 3-PG (0 – 10mM), similar to the assay for GAPDH described above.

Phosphosglycerate Mutase: The forward reaction was coupled to ENO, PK and LDH in the presence of 2,3-BPG (2 mM), NADH (1 mM) and initialised with varying concentrations of 3-PG (0 – 10 mM). The reverse reaction converting 2-PG (0 – 20 mM) to 3-PG was coupled to PGK and GAPDH in the presence of ATP (4 mM), NADH (1 mM) and 2,3-BPG (2 mM).

Enolase: The forward direction was assayed by linking the reaction to PK and LDH in the presence of co-factors, NADH (1 mM) and ADP (4 mM). The reaction was initialised by varying concentrations of 2-PG (0 – 20 mM).

Pyruvate Kinase: Characterisation of the enzyme was performed in the forward direction by coupling the reaction to LDH in the presence of NADH (1 mM) serving as the indicator reaction, and varying the ADP (0 – 30 mM) or PEP (0 – 20 mM) concentration. Inhibition by PEP and ATP (0 – 5 mM) was also determined.

Lactate Dehydrogenase: The forward reaction was assayed by varying either NADH (0 – 1 mM) or pyruvate (0 – 20 mM). Characterisation of the reverse reaction was achieved through reduction of NAD^+ in presence of varying concentration of either NAD^+ (0 – 1 mM) or LAC (0 – 120 mM).

3.4.2 Fitting to kinetic data

A mechanistic rate equation that describes a particular enzyme′s kinetics was fitted to all the kinetic data collected from its isolated experimental characterisation assays. Experiments were conducted to determine the substrate and product affinity constants for each enzyme. Fitting was performed using the `NonlinearModelFit` function in Wolfram Mathematica ver. 12.

3.5 Model construction and simulation

The MDA-mb-231 model was constructed using Wolfram Mathematica ver. 12. Fitted rate equations were incorporated into ordinary differential equations (ODEs) and the `NDsolve` function was used to solve these ODEs.

3.6 Flux analysis assay

Glycolytic flux determination was conducted on whole MDA-mb-231 and MCF-7 cells. The change in extracellular glucose and lactate concentrations over time was used to calculate the flux through glycolysis. Cells were grown to ± 80% confluence according to culturing protocol previously mentioned (Section 3.1). The media was decanted, washed and replaced with low-glucose (1 mg/mL glucose) DMEM. Growth media samples were collected (0.5 mL) from T175 cm^3 flasks (*Nest*) over the course of 0 – to – 9 hours. Immediately thereafter, cells were harvested and both the flux and cell protein samples were stored at -20°C. Glucose and lactate determination assays were conducted on flux samples collected. A hexokinase-G6PDH coupled assay was performed to

determine the glucose concentration by converting glucose to G6P and subsequently, G6P to 6-PG through the reduction of $NADP^+$ via Hexokinase and G6PDH, respectively. Assay mixture (0.1 TRIS/HCl buffer pH ± 8.0, 2 mM mg.ATP, 4 mM $NADP^+$, 4 mM $MgCl_2$, 20 U/ml hexokinase, 25 U/mL G6PDH) was added to flux samples and the absorbance was read spectrophotometrically at 340 nm. For lactate determination assays, LDH was utilized to convert lactate into pyruvate by reduction of NAD^+. The reaction mixture that was added to the flux sample contained 1 x PBS, 5 mM NAD^+, 12.5 U/mL LDH and 2.5% v/v Hydrazine. Both glucose and lactate determination assays were measured spectrophotometrically at 340 nm and data was normalised to mg.total protein, which was determined by performing a Bradford determination assay.

3.7 ^{14}C – glucose isotopic labelling experiment

MDA-mb-231 cells were cultured and maintained as previously described (Section 3.1), however the harvesting protocol was modified, with cells being resuspended in assay buffer (0.1 M Tris pH 7.0, 15 mM NaCl, 0.14 mM KCl, 0.5 mM $CaCl_2$) supplemented with 1 mM DTT and 1 mM PMSF. The lysate was prepared as described in Section 3.2. Thereafter, a pre-test on harvested lysate was conducted to determine viability and glucose time-dynamics to establish cytosolic reaction sampling times. For the test, lysate was mixed with sampling buffer and supplemented with 1 mM PMSF, 1 mM DTT, 5 mM phosphate buffer and 2.5 mM $MgSO_4$ and pre-heated to 37°C before initialising with substrate and co-factors (final concentration of 1 mM Glc, 2 mM ATP and 1 mM NAD^+). Once lysate viability and glucose time-dynamics were determined the ^{14}C-glucose isotopic labelling assay was performed. The remaining lysate (5 mg of protein) was mixed with sample buffer (1 mM PMSF, 1 mM DTT, 5 mM phosphate buffer and 2.5 mM $MgSO_4$) and pre-heated to 37°C. Thereafter, glycolysis was initialised with a mixture of 0.5 mM ^{14}C-glucose (*AEC Amersham*), 0.5 mM unlabelled glucose, 2 mM ATP, 1 mM NAD^+. Upon initialising the reaction, a cell sample was withdrawn (time 0) and subsequent cell samples were withdrawn at appropriate time points as determined by glucose time-dynamics. Immediately thereafter samples were thoroughly mixed with perchloric acid (final concentration of ± 9% v/v) and placed on ice for 10 min before being neutralized with 1 M K_2CO_3 and centrifuged at 20 817 RCF for 15 min at 4°C. The supernatant was collected and stored at -20°C until HPLC analysis, to determine the change in metabolites and co-factors over the various time samples collected.

3.7.1 Ion-Pairing Reverse High Performance Liquid Chromatography

We used an in-house developed Ion-Pairing Reverse HPLC method to quantify ^{14}C-glycolytic intermediates and co-factors in MDA-mb-231 cells, to validate the constructed glycolytic model. For this a liquid chromatography (*SpectraSYSTEM* HPLC) system was coupled in series to the *SpectraSystem* UV6000LP UV-Vis and *LabLogic* β-RAM model 5 radiolabelled detector. A reverse phase Phenomenex Luna C_{18} column (5 μm) was utilised to separate metabolites. Mobile phase A (MPA) was 25 mM tetrabutyl ammonium bisulfate in water adjusted to a pH of 7.3 ($\pm$ 1), and mobile phase B (MPB) was 2.5% v/v water in acetonitrile. The injection volume for all samples was 10 μL. A linear gradient was utilized as follows: 0 – 4.5 min, 95% MPA and 5% MPB; 5 – 12 min 70% MPA and 30% MPB; 13 – 20 min 95% MPA and 5% MPB. The flow rate was 1 mL/min for the total run time of 20 min. Column effluent was measured at 254 nm by UV-Vis detector and thereafter mixed with scintillation fluid in a 3:1 ratio for the radiolabelled detector. The radiolabelled detector then initiated measurement 1 min after injection and terminated at a runtime of 13 min.

3.7.2 Quantification of glycolytic intermediates and co-factors

The peaks of co-factors and glycolytic intermediates were quantified via UV-Vis detector and linked radiolabelled detector, respectively. The radiolabelled detector generated a chromatographic trace for each time sample, as shown in Figure 3.1(a). Each chromatographic trace was quantified to determine the concentrations from the peak areas as the peaks represent the separated metabolites. The peak area was estimated by fitting a skewed Gaussian function using the `NonlinearFit` function in Mathematica, as depicted in Figure 3.1(b). This provided a means to quantify the peak areas and determine the response factor from the initiating ^{14}C-glucose and unlabelled glucose, and to calculate the concentration of metabolites from the appropriate peak in each chromatographic trace.

In contrast, co-factor metabolites peaks were quantified using the UV-Vis detector at 253 nm (see Fig. 3.2(a)). Calibration curves for each co-factor metabolite (ATP, ADP, AMP, NAD^+ and NADH) were prepared in assay buffer under the same condition as the samples (50% PCA treatment, 1 M K_2CO_3 neutralisation and centrifugation) to accurately determine the concentrations present in the eluent. Calibration standards for co-factor metabolites were prepared by a dilution series over a 2.0-to-0.031 mM range. The area under the peak was determined for the co-factors in each chromatographic trace using the `ChromSolve` software tool that is linked to the HPLC analysis software kit. The area under the peak was plotted against the concentration to

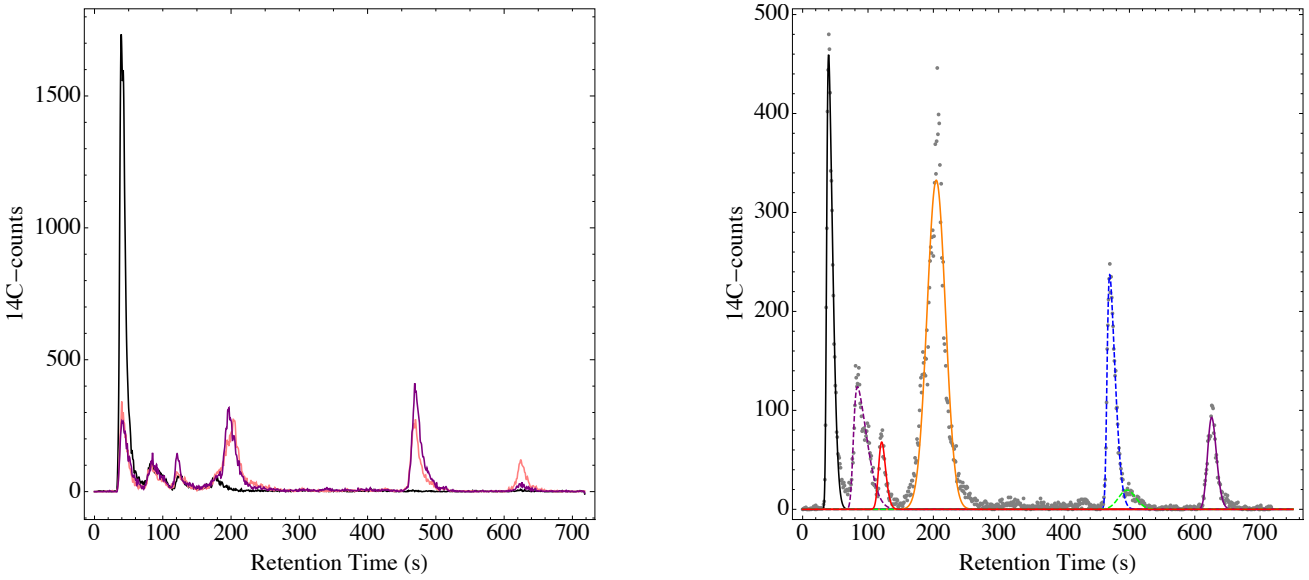

(a) (b)

Figure 3.1: (a) Chromatographic traces of the time-dependent change in ^{14}C-labelled glycolytic intermediates observed by the radiolabelled detector. Each colour represents a chromatographic trace at a specific time point where, 0 min (Black), 30 min (Pink) and 60 min (Purple). (b) Determination of the peak areas in a chromatographic trace at time 10 min by employing the skewed Gaussian distribution and `NonlinearFit` functions in Wolfram Mathematica. Each peak depicts a metabolite that was detected via the *LabLogic* β-RAM model 5 radiolabelled detector. Metabolites shown are GLC (Black), F16BP(Purple), DHAP (Orange), 3-PG (Dashed Blue), 2-PG (Dashed Green), LAC (Red) and an impurity from the labelled ^{14}C-glucose (Dashed Purple).

generate the calibration curve as shown in Fig. 3.2(b). The calibration curves were utilised to quantify the change in co-factor concentrations over time in the samples via the UV-Vis detector.

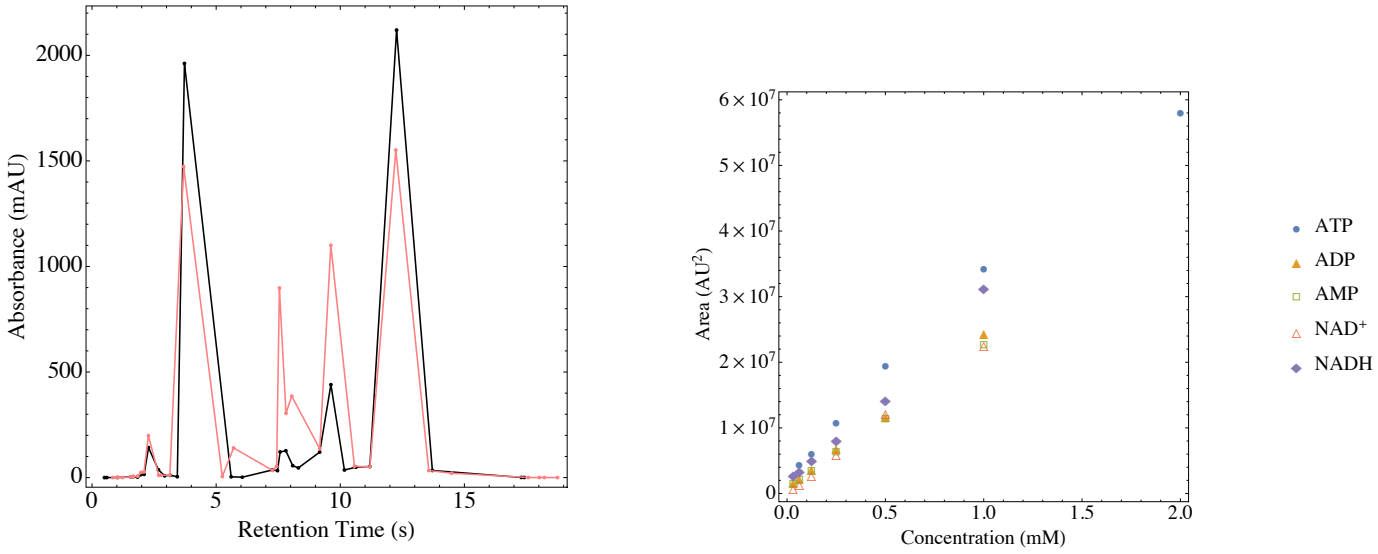

(a) (b)

Figure 3.2: (a) An example of the chromatographic trace for the adenosine and nicotinamide species. Each colour represents a chromatographic trace at a specific time point: 0 min (Black) and 15 min (Pink). (b) Description of the calibration standards measured by the UV-Vis detector (254 nm) to quantify the concentration of co-factors in the samples. Co-factor standards were prepared at known concentrations ranging from 1 mM to 0.031 mM for ADP, AMP, NAD^+ and NADH, whereas ATP ranged from 2 mM to 0.063 mM.

Chapter 4

Results and discussion: Enzyme Characterisation and Model construction

This chapter presents the results for characterising all glycolytic enzymes and constructing a mathematical model of glycolysis in MDA-mb-231. Coupled enzymes assays were performed to obtain kinetic datasets of each enzyme, which were used to fit to a single mechanistic rate equation – describing that particular enzyme's kinetics. Wolfram Mathematica 12 was employed to fit the rate equation to the dataset(s). All glycolytic enzymes were characterised, as well as AK and LDH. Fitting a rate equation on the dataset of each enzyme yields parameter values required for model construction. Hereafter, the rate equations and parameter values are combined into ODEs with each ODE describing the rate of change of a glycolytic metabolite.

4.1 MDA-mb-231: Glycolytic enzyme characterisation

4.1.1 Hexokinase

Hexokinase catalyses the phosphorylation of glucose by ATP to glucose-6 phosphate and ADP. The forward specific activity and affinity constants for ATP, ADP, AMP and glucose were characterised. Hexokinase showed ADP product inhibition as well as AMP inhibition, however, the concentrations of ADP and AMP required are above 10 mM, which is much higher than the physiological concentration. Furthermore, hexokinase is an essentially irreversible reaction, due to its high K_{eq} of 3800 [9], and the kinetic data were based upon an irreversible rate equation (Eq. 4.1). The resulting fit is shown in Fig. 4.1 and the parameter values obtained from the fit are listed in Table 4.1. G6P product inhibition was not determined due to limitations of the coupled assay method used. Isolating the enzyme from the lysate would solve the problem, but falls beyond the scope of this thesis.

$$vHK = \frac{\mathrm{Vmf}.\frac{\mathrm{atp}}{\mathrm{Katp}}.\frac{\mathrm{glc}}{\mathrm{Kglc}}}{(1+\frac{\mathrm{glc}}{\mathrm{Kglc}})\cdot(1+\frac{\mathrm{atp}}{\mathrm{Katp}}+\frac{\mathrm{adp}}{\mathrm{Kiadp}})\cdot(1+\frac{\mathrm{amp}}{\mathrm{Kiamp}})} \tag{4.1}$$

Table 4.1: Kinetic parameters for hexokinase in MDA-mb-231. Fitted an irreversible bi-substrate Michaelis-Menten (Eq. 4.1) to the experimental data and the parameters obtained are shown with mean ± SE.

Parameter	Fitted Value	Literature Value	References
$V_{f\,HK}$(μmol.min^{-1}.mg^{-1} protein)	0.057 ± 0.0027	0.13 ± 0.001[1]	[48]
K_{GLC}(mM)	0.096 ± 0.017	0.1[2]	[8]
K_{ATP}(mM)	0.89 ± 0.14	1.1[2]	[8]
$K_{i\ ADP}$(mM)	24 ± 8.8	-	-
$K_{i\ AMP}$(mM)	8.9 ± 2.1	-	-

[1]Specific activity from Bcap37 breast cancer carcinoma cells
[2]Affinity constants determined in HeLa cells

The specific activity of hexokinase in MDA-mb-231 is 2-fold lower than that of the Bcap37 breast cancer cell line, but the affinity constants were comparable to those in HeLa cells. The majority of cancer cells express the HKI and HKII isoforms and, therefore it was deemed appropriate to compare the affinity constants of MDA-mb-231 cells to HeLa cells, despite the differences in their metabolic profiles [53].

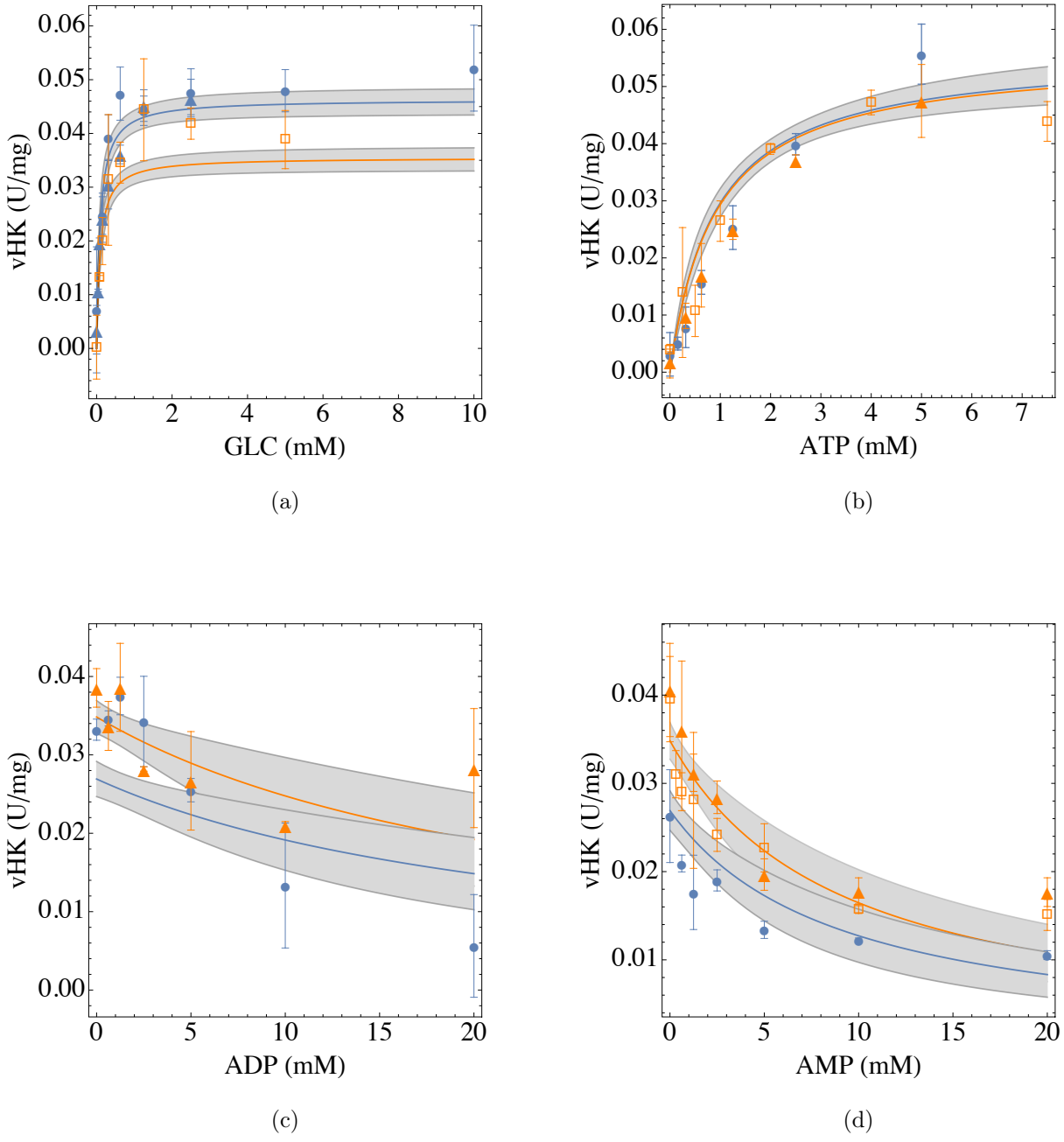

Figure 4.1: Characterisation of kinetic parameters of hexokinase (HK) in MDA-mb-231 cells. The hexokinase maximal forward activity and affinity constants were characterised by fitting a bi-substrate irreversible rate equation (Eq. 4.1) to the kinetic data. Each panel and symbol (circle, square and triangle) represent a biologically independent experiment. The blue and orange curves indicate the fits to kinetic data of two different conditions. Grey bands indicate 95% confidence prediction intervals. The HK activity for (a) varying GLC was measured at 4 mM (blue) and 1.5 mM (orange) ATP, (b) varying ATP at 10 mM (blue) and 5 mM (orange) GLC, ADP inhibition of HK (c) was measured at 1.5 mM ATP and 0.3 mM (blue) or 5 mM (orange) GLC, HK inhibition by AMP (d) was also measured at 1.5 mM ATP and 0.3 mM (blue) or 5 mM (orange) GLC. Error bars indicate SD of the technical triplicates.

4.1.2 Phosphoglucoisomerase

Phosphoglucoisomerase catalyses a reversible reaction that converts glucose-6 phosphate to fructose-6 phosphate. The forward and reverse rate kinetics as well as the affinity constants (K_{G6P} and K_{F6P}) in PGI were characterised. Both datasets demonstrated classic Michaelis-Menten behaviour that was fitted to using a uni-uni reversible rate equation (Eq. 4.2). The upper and lower limits of the K_{eq} were calculated using the Haldane relation and it was established that the equilibrium constant in MDA-mb-231 breast cancer cell is greater than in reported literature [9]. The large variation between two independent experiments for the forward direction, Fig. 4.2 (a), probably contributes to the large range for the estimated K_{eq}. More kinetic data would likely narrow the K_{eq} range and might bring the value closer to the K_{eq} found in the literature. Table 4.2 shows the values obtained from the fit.

$$vPGI = \frac{\mathrm{Vmf} \cdot \frac{\mathrm{g6p}}{\mathrm{Kg6p}} - \mathrm{Vmr} \cdot \frac{\mathrm{f6p}}{\mathrm{Kf6p}}}{1 + \frac{\mathrm{f6p}}{\mathrm{Kf6p}} + \frac{\mathrm{g6p}}{\mathrm{Kg6p}}} \tag{4.2}$$

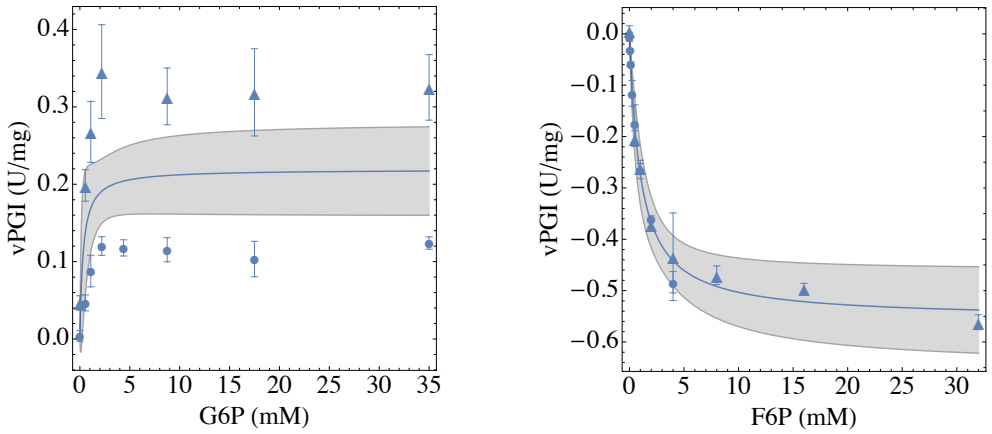

(a) (b)

Figure 4.2: Kinetic parameter characterisation of phosphoglucoisomerase in MDA-mb-231 cells. Assays were conducted to determine the maximal forward and reverse specific activity and the affinity constants (K_{G6P} and K_{F6P}) by fitting an uni-uni Michaelis-Menten rate equation to the kinetic data. Panel (a) and (b) represent the forward and reverse reaction, respectively. Both panels were determined for independent experiments and display two independent experiments shown by the symbols (disc and triangle). The saturation curves are shown with 95% confidence prediction interval (grey region) and error bars indicate SD of the technical triplicate data.

Table 4.2: An overview of the kinetic parameters characterised for phosphoglucoisomerase in MDA-mb-231. The assayed data were fitted to using a uni-uni reversible rate equation (Eq. 4.2) to determine the parameters for the forward and reverse reactions. Values are given as mean ± SE.

Parameter	Fitted Value	Literature Value	References
$V_{f\ PGI}$(μmol.min^{-1}.mg^{-1} protein)	0.22 ± 0.029	1.2 ± 0.20[2]	[8]
$V_{r\ PGI}$(μmol.min^{-1}.mg^{-1} protein)	0.55 ± 0.046	0.86 ± 0.42[1]	[48]
K_{G6P}(mM)	0.32 ± 0.30	0.4 ± 0.03[2]	[8]
K_{F6P}(mM)	1.0 ± 0.30	0.05[2]	[8]
K_{eq}(mM)	0.87 - 15	0.314	[9]

[1]Specific activity from Bcap37 breast cancer carcinoma cells
[2]Determined in HeLa cells

4.1.3 Phosphofructokinase

Phosphofructokinase catalyses the phosphorylation of fructose-6 phosphate by ATP to fructose-1,6-bisphosphate. Substrate inhibition by ATP was observed in all the saturation curves varying ATP concentrations. However, higher F6P concentrations can decrease the enzyme′s sensitivity to ATP inhibition. Additionally, the binding coefficients of ADP and AMP were also characterised and found that PFK is sensitive to ADP and AMP inhibition. A modified irreversible bi-substrate Michaelis-Menten rate equation was used to describe PFK kinetics. The parameters obtained from the fit are shown in Table 4.3 and Fig. 4.3 shows the resulting fits and the kinetic data. However, the rate equation was unable to fully characterise the role F6P plays in ATP inhibition. The affinity constant for F16BP could not be accurately determined in cell lysate. To characterise the different states of the enzymes′ subunits and cooperative binding would require the MWC equation, which would probably produce a better fit, especially for ATP, but would require a more complete kinetic characterisation. For the current study, the following equation was used:

$$vPFK = \frac{\mathrm{Vmf}\cdot\frac{\mathrm{atp}\cdot\mathrm{f6p}}{\mathrm{Katp}\cdot\mathrm{Kf6p}}}{(1+\frac{\mathrm{f6p}}{\mathrm{Kf6p}})\cdot(1+\frac{\mathrm{atp}}{\mathrm{Katp}}+\frac{\mathrm{adp}}{\mathrm{Kadp}})\cdot(1+\frac{\mathrm{amp}}{\mathrm{Kiamp}}+\frac{\mathrm{atp}}{\mathrm{Kiatp}}+\frac{\mathrm{atp}^2}{\mathrm{Kiatp}^2})} \tag{4.3}$$

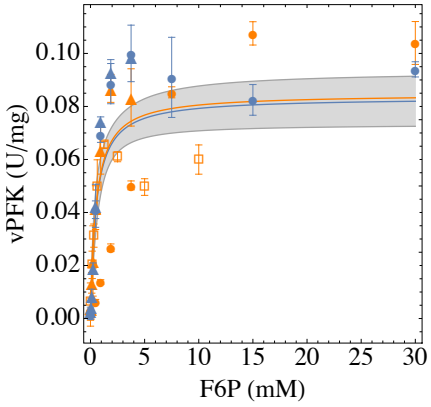

(a)

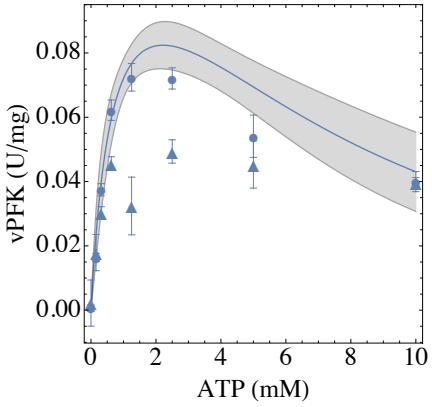

(b)

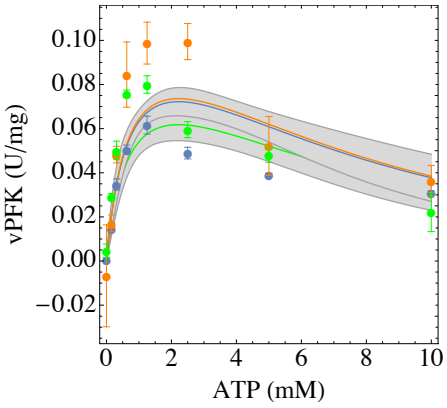

(c)

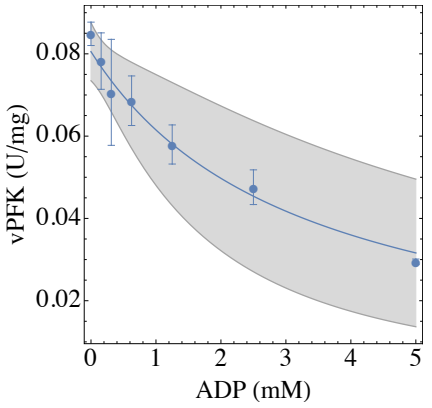

(d)

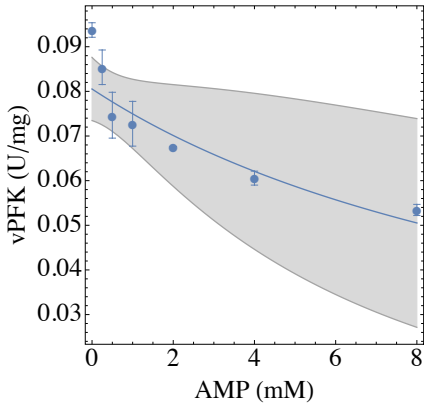

(e)

Figure 4.3: Continues on the following page.

Figure 4.3: Kinetic parameter characterisation of phosphofructokinase in MDA-mb-231 cells. Enzyme assays were conducted to determine the maximal specific rate and binding coefficients for substrates ATP and F6P as well as inhibition constants (ATP, ADP and AMP). The irreversible bi-substrate Michaelis-Menten rate equation was fitted to all the kinetic data to obtain the parameters in Table 4.3. Each panel and symbol represents an independent experiment. The coloured curves (blue, orange and green) shown indicate the different experimental conditions, and the grey region depicts the 95% confidence prediction intervals. Error bars indicate SD of the technical triplicate. The PFK activity was determined in panel (a) by varying F6P concentrations at 4 mM (blue) and 1.25 mM (orange) ATP; in panel (b) by varying ATP concentrations at 5mM F6P. In the case of panel (c) ATP concentrations were varied at 2 mM (blue), 2.2 mM (orange) and 1.1 mM (green) F6P. For PFK inhibition by ADP and AMP in panels (d) and (f), respectively, the inhibitor was varied at 10 mM F6P and 1.25 mM ATP.

Table 4.3: An overview of kinetic parameters obtained experimentally for phosphofructokinase in MDA-mb-231 breast cancer cells. The PFK enzymatic data was fitted using a bi-substrate Michaelis-Menten rate equation to obtain parameters listed below. Values given as mean ± SE.

Parameter	Fitted Value	Literature Value	References
$V_{f\,PFK}$(μmol.min^{-1}.mg^{-1} protein)	0.16 ± 0.033	0.033 ± 0.010[1]	[40]
K_{F6P} (mM)	0.52 ± 0.12	1.03 ± 0.26[1]	[40]
K_{ATP}(mM)	0.77 ± 0.33	0.010 ± 0.03[1]	[40]
$K_{i\ ATP}$(mM)	9.8 ± 2.9	-	-
$K_{i\ ADP}$(mM)	1.2 ± 0.67	-	-
$K_{i\ AMP}$(mM)	12 ± 7.7	-	-

[1] Determined from MCF-7 breast carcinoma cells

MDA-mb-231 exhibits a more aggressive glycolytic phenotype than MCF-7 cancer cells and the PFK activity being 5-fold higher in the former cell line indicates a significantly higher PFK expression. Zancan *et al.* [41] demonstrated that the two cell lines possess a similar PFK isoform expression pattern.

4.1.4 Aldolase

Aldolase catalyses a reversible reaction that cleaves F16BP into GAP and DHAP. The enzyme's binding coefficient for F16BP and forward specific activity were characterised by fitting a uni-bi Michaelis-Menten equation (Eq. 4.4) to the enzymatic kinetics of aldolase. Table 4.4 shows the parameter values obtained from the fit and Fig. 4.4 illustrates the fitted kinetic data. It was not possible to measure the reaction in reverse direction and literature values were used for product inhibition and K_{eq}. When compared to HeLa cells, a much lower specific activity for aldolase was observed in the MDA-mb-231 cells. This is surprising given its higher flux value.

$$vALD = \frac{\mathrm{Vmf} \cdot \frac{\mathrm{f16bp}}{\mathrm{Kf16bp}} \cdot \left(1 - \frac{\mathrm{dhap \cdot gap}}{\mathrm{f16bp \cdot Keq}}\right)}{\frac{\mathrm{dhap \cdot gap}}{\mathrm{Kdhap \cdot Kgap}} + \frac{\mathrm{dhap}}{\mathrm{Kdhap}} + \frac{\mathrm{f16bp}}{\mathrm{Kf16bp}} + \frac{\mathrm{gap}}{\mathrm{Kgap}} + 1} \tag{4.4}$$

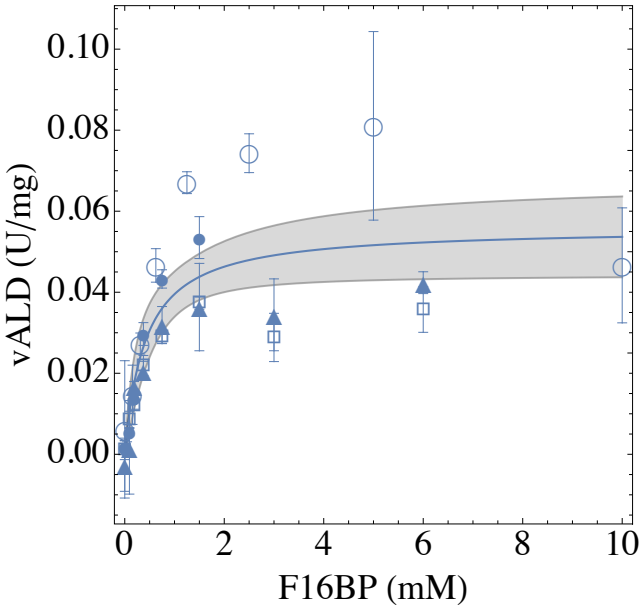

Figure 4.4: Kinetic parameter characterisation of aldolase in MDA-mb-231 cell extract. The aldolase maximal specific forward activity and affinity constant for F16BP were determined by fitting a rate equation (Eq. 4.4) to the kinetic data. The symbols (filled and empty disc, triangle and square) indicate four independent experiments. Data points and the grey region represent mean ± SD of technical repeats and 95% confidence prediction interval, respectively.

Table 4.4: Overview of kinetic parameters for aldolase in MDA-mb-231. The kinetic parameters were characterised by fitting an uni-bi Michaelis-Menten equation to experimental data. Values shown as the mean ± SE.

Parameter	Fitted Value	Literature Value	References
$V_{f\ ALD}$(μmol.min^{-1}.mg^{-1} protein)	0.056 ± 0.0057	0.20 ± 0.002[1]	[48]
K_{F16BP}(mM)	0.41 ± 0.15	0.009[3]	[8]
K_{GAP}(mM)	-	0.16[2]	[8]
K_{DHAP}(mM)	-	0.08[2]	[8]
K_{eq}(mM)	-	0.069	[9]

[1]Specific activity from Bcap37 breast cancer carcinoma cells
[2]Affinity constants determined in rat AS-30D hepatoma cells
[3]Affinity constants measured in HeLa cells

4.1.5 Triosephosphate Isomerase

Triosephosphate isomerase catalyses a reversible reaction that interchangeably converts DHAP to GAP. The reverse maximal activity and affinity constant (K_{GAP}) of TPI was characterised. No data was collected for the forward reaction. Kinetics of TPI reaction were fitted to the reversible uni-uni Michaelis-Menten rate equation (Eq. 4.5). Taking literature values for the parameters for which no experimental data would be obtained, as shown in Table 4.5. The activity of TPI displays a typical saturation kinetics (in Fig. 4.5).

$$vTPI = \frac{\mathrm{Vmr} \cdot \frac{\mathrm{gap}}{\mathrm{Kgap}}\left(\frac{\mathrm{dhap}\cdot\mathrm{Keq}}{\mathrm{gap}} - 1\right)}{\frac{\mathrm{dhap}}{\mathrm{Kdhap}} + \frac{\mathrm{gap}}{\mathrm{Kgap}} + 1} \tag{4.5}$$

Table 4.5: Overview of kinetic parameters for triosephosphate in MDA-mb-231 cells. A reversible uni-uni Michaelis-Menten equation was fitted to all the kinetic data to obtain the kinetic parameters listed below. Values are shown as mean ± SE.

Parameter	Fitted Value	Literature Value	References
$V_{r\ TPI}$(μmol.min^{-1}.mg^{-1} protein)	1.7 ± 0.29	3.2 ± 0.12[1]	[48]
K_{GAP}(mM)	1.2 ± 0.52	0.51	[8]
K_{DHAP}(mM)	-	1.6	[8]
K_{eq}(mM)	-	0.045	[9]

[1]Determined in Bcap37 breast cancer cells
[2] Affinity constants determined in HeLa cells

The specific activity and affinity constant are lower than for the TPI found in HeLa cells. It is unclear why the enzyme is found to be different between the two cell lines, as TPI serves the purpose of preventing the build-up of DHAP that can be converted to methylglyoxal, which would be detrimental to cancer

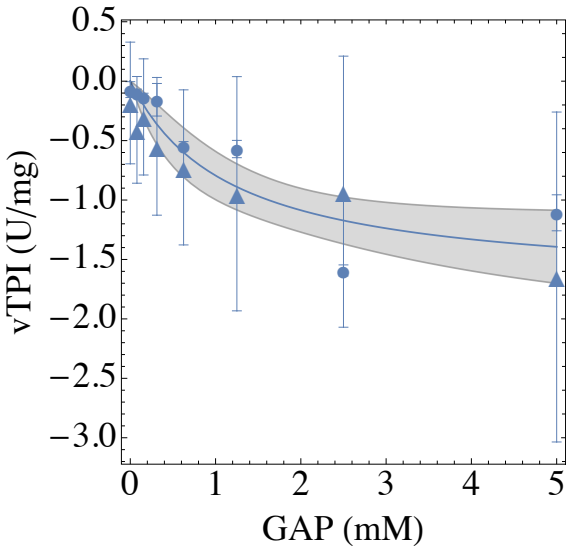

(a)

Figure 4.5: Kinetic characterisation of triosephosphate isomerase in MDA-mb-231 cells. The enzyme's maximal specific reverse activity and binding coefficient for GAP were characterised by fitting the rate equation (Eq. 4.5) to the kinetic data. Panel represents two independent experiments. Error bars are SD of technical triplicates. Model fits are shown with 95% confidence prediction interval bands (grey region).

cells [49]. However, the activity of TPI is high compared to that of the other enzymes and the reaction is probably close to equilibrium in the system, and therefore not limiting the flux.

4.1.6 Glyceraldehyde 3-Phosphate Dehydrogenase

Glyceraldehyde 3-phosphate dehydrogenase catalyses the reaction of glyceraldehyde 3-phosphate and NAD^+ to 1,3-bisphosphoglycerate and NADH. The maximal reverse specific activity for GAPDH was characterised by coupling the reaction to PGK, which is necessary due to the instability of B1,3PG. In this assay, the PGK conversion of 3-PG to B1,3PG is assumed to take place at equilibrium. By using the PGK K_{eq} of 3200 [9], it was possible to calculate the concentration of B1,3PG from the initial 3-PG and ATP concentrations. A reversible bi-substrate Michaelis-Menten kinetics equation (Eq. 4.6) was used to fit the GAPDH kinetic data (displayed in Fig. 4.6). Table 4.6 shows the parameters obtained from the fit. Due to the large difference in maximal activity for the B1,3PG and NADH saturation curve, no good overall fit for both experiments was possible. For the forward reaction specific activity of GAPDH and affinity constants (K_{GAP} and K_{NAD^+}) from the Bcap37 breast cancer and HeLa cells were used, respectively.

$$vGAPDH = \frac{\mathrm{Vmf} \cdot \frac{\mathrm{gap \cdot nad}}{\mathrm{Kgap \cdot Knad}} - \mathrm{Vmr} \cdot \frac{\mathrm{b13pg \cdot nadh}}{\mathrm{Kb13pg \cdot Knadh}}}{\left(\frac{\mathrm{b13pg}}{\mathrm{Kb13pg}} + \frac{\mathrm{gap}}{\mathrm{Kgap}} + 1\right)\left(\frac{\mathrm{nad}}{\mathrm{Knad}} + \frac{\mathrm{nadh}}{\mathrm{Knadh}} + 1\right)} \tag{4.6}$$

Table 4.6: An overview of kinetic parameters for glyceraldehyde 3-phosphate dehydrogenase in MDA-mb-231 cells. The parameters were obtained by fitting the rate equation (Eq. 4.6) to the kinetic data. Values shown represent mean ± SE.

Parameter	Fitted Value	Literature Value	References
$V_{f\,GAPDH}$(μmol.min^{-1}.mg^{-1} protein)	-	1.0 ± 0.038[1]	[48]
$V_{r\,GAPDH}$(μmol.min^{-1}.mg^{-1} protein)	0.45 ± 0.11	-	-
$K_{B1,3PG}$(mM)	0.029 ± 0.018	-	-
K_{NADH}(mM)	0.15 ± 0.13	0.01	[8]
K_{GAP}(mM)	-	0.19[2]	[8]
K_{NAD^+}(mM)	-	0.09[2]	[8]

[1] Determined in Bcap37 breast cancer cells
[2] Affinity constants determined in HeLa cells

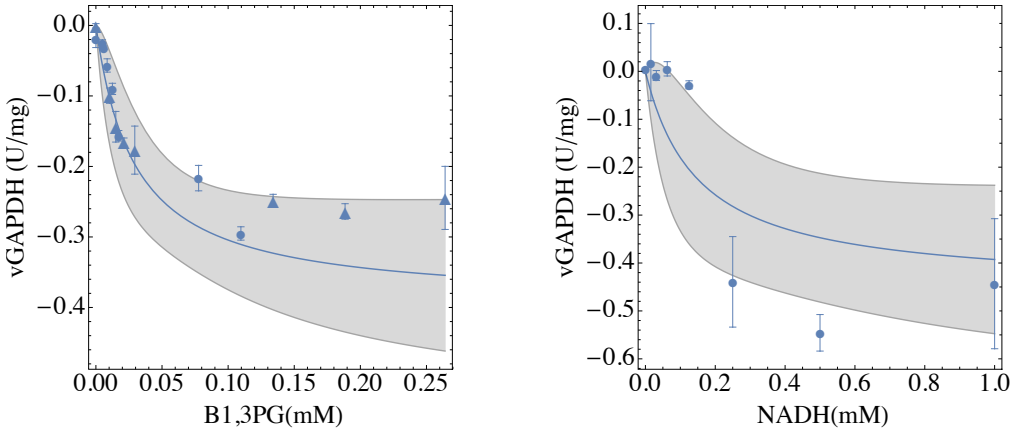

(a) (b)

Figure 4.6: Kinetic characterisation of glyceraldehyde 3-phosphate in MDA-mb-231 cells. Fitted a mechanistic bi-substrate rate equation to the kinetic data to characterise the maximal reverse specific activity and the binding coefficients for NADH and B1,3PG. The B1,3PG concentrations were derived by using the PGK K_{eq} and the initial 3-PG and ATP concentrations. Panels (a) and (b), and symbols (disc and triangle) represent independent experiments. Error bars on kinetic data is SD of technical triplicates and grey regions shown are the 95% confidence prediction interval. The assay in panel (a) was performed by varying 3-PG at 1 mM NADH and in panel (b) by varying NADH at 10 mM 3-PG.

4.1.7 Phosphoglycerate Kinase

Phosphoglycerate kinase catalyses the reversible conversion of 1,3-bisphosphate and ADP to glycerate 3-phosphate and ATP via the transfer of a phosphate group. PGK was assayed in the reverse direction to determine the binding affinities (K_{ATP} and $K_{3\text{-}PG}$) and maximal specific activity. Fitted a random bi-substrate bi-product rate equation (Eq. 4.7) to the experimental data, the parameters obtained are shown in Table 4.7 and Fig. 4.7 shows the resulting fits and kinetic data. The binding constant for reverse reaction by ADP was not determined.

$$vPGK = \frac{\mathrm{Vmr} \cdot \frac{\mathrm{atp{\cdot}3pg}}{\mathrm{Katp{\cdot}K3pg}} \left(\frac{\mathrm{adp{\cdot}b13pg{\cdot}Keq}}{\mathrm{atp{\cdot}3pg}} - 1 \right)}{\left(\frac{\mathrm{adp}}{\mathrm{Kadp}} + \frac{\mathrm{atp}}{\mathrm{Katp}} + 1 \right) \left(\frac{\mathrm{b13pg}}{\mathrm{Kb13pg}} + \frac{\mathrm{3pg}}{\mathrm{K3pg}} + 1 \right)} \tag{4.7}$$

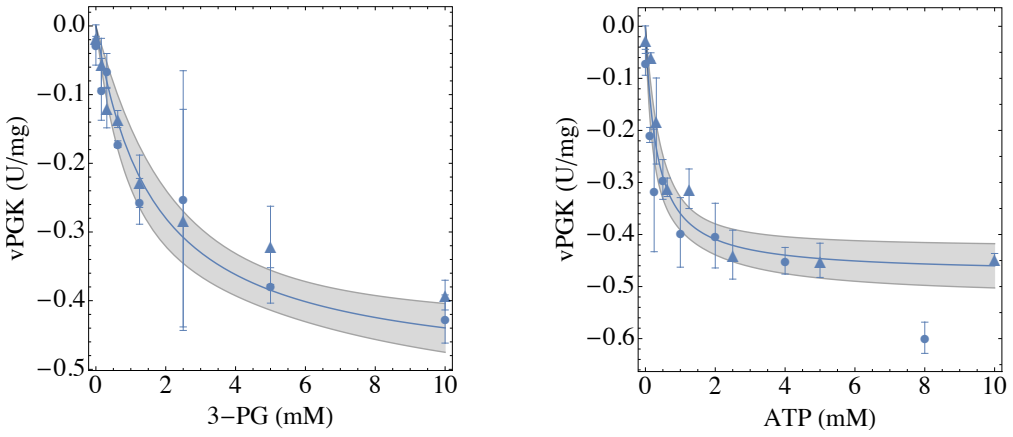

(a) (b)

Figure 4.7: Kinetic characterisation of phosphoglycerate kinase in MDA-mb-231. Fitted the bi-substrate Michaelis-Menten rate equation (Eq. 4.7) to the experimental data to obtain maximal specific reverse activity and binding affinities for ATP and 3-PG. Each panel and symbol shown is an independent experiment that was fitted and displayed with 95% confidence prediction interval. Error bars represent SD of the technical triplicates. PGK activity in panel (a) was determined at 4 mM ATP and in panel (b) at 10 mM 3-PG.

Table 4.7: Overview of kinetic parameters for phosphoglycerate kinase in MDA-mb-231 cell extract. Fitted the Michaelis-Menten equation (Eq. 4.7) to the experimental kinetic data to obtain the parameters shown below as mean ± SE.

Parameter	Fitted Value	Literature Value	References
$V_{r\ PGK}$(μmol.min^{-1}.mg^{-1} protein)	0.55 ± 0.040	-	-
$K_{3\text{-}PG}$(mM)	1.7 ± 0.42	0.13	[8]
K_{ATP}(mM)	0.32 ± 0.079	0.27	[8]
K_{B13PG}(mM)	-	0.079[1]	[8]
K_{ADP}(mM)	-	0.04[1]	[8]
K_{eq}	-	3200	[9]

[1]Determined in HeLa cervical cancer cells

4.1.8 Phosphoglycerate Mutase

Phosphoglycerate mutase is the 8th step in glycolysis and catalyses the isomerisation of 3-phosphoglycerate to 2-phosphoglycerate. PGM is a reversible reaction, and the forward and reverse maximal specific activity as well as the affinity constants ($K_{3\text{-}PG}$ and $K_{2\text{-}PG}$) were characterised (listed in Table. 4.8). Both the forward and reverse reaction displayed classic Michaelis-Menten saturation curves for 3-PG and 2-PG, as shown in Fig. 4.8. The kinetics for PGM were described by a mono-substrate reversible Michaelis-Menten equation (Eq. 4.8). The PGM of MDA-mb-231 was found to be 2,3-bisphosphoglycerate (2,3-BPG) co-factor dependent. Varying 2,3-BPG concentrations in a PGM coupled enzyme assay generated a hyperbolic saturation curve (in Appendix A.1). In all PGM kinetic assays we used a saturating 2,3-BPG concentration of 2.0 mM.

$$vPGM = \frac{\mathrm{Vmf} \cdot \frac{\mathrm{p3g}}{\mathrm{K3pg}} - \mathrm{Vmr} \cdot \frac{\mathrm{p2g}}{\mathrm{K2pg}}}{\frac{\mathrm{p2g}}{\mathrm{K2pg}} + \frac{\mathrm{p3g}}{\mathrm{K3pg}} + 1} \tag{4.8}$$

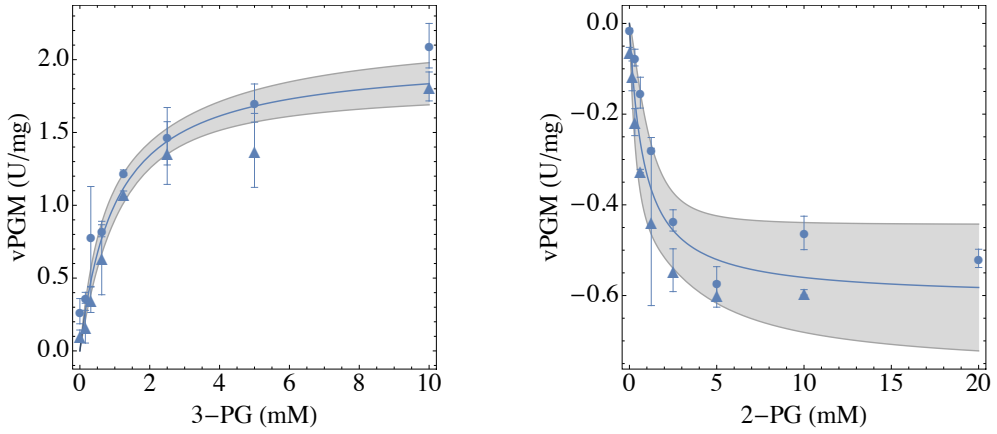

(a) (b)

Figure 4.8: Kinetic characterisation of phosphoglycerate mutase in MDA-mb-231. Parameters were calculated by fitting the mechanistic rate equation (Eq. 4.8) to the kinetic data. The forward and reverse reactions were assayed independently, which is shown by panels (a) and (b) respectively. Furthermore, each symbol represents an independent experiment. Errors bars are SD of the technical triplicates. In addition, fits shown are depicted with a 95% (grey region) confidence prediction interval.

Table 4.8: An overview of kinetic parameters for phosphoglycerate mutase in MDA-mb-231 cells. The forward and reverse activity, including the affinity constants were characterised by fitting the rate equation (Eq. 4.8) to the kinetic data to obtain the parameters listed in the table below. Values are given as mean ± SE.

Parameter	Fitted Value	Literature Value	References
$V_{f\,PGM}$(μmol.min^{-1}.mg^{-1} protein)	2.0 ± 0.10	1.4[1]	[8]
$V_{r\,PGM}$(μmol.min^{-1}.mg^{-1} protein)	0.61 ± 0.079	0.53[1]	[8]
$K_{3\text{-}PG}$(mM)	1.0 ± 0.17	0.19[1]	[8]
$K_{2\text{-}PG}$(mM)	0.82 ± 0.41	0.12[1]	[8]

[1]Determined in HeLa cells

4.1.9 Enolase

Enolase catalyses the conversion of 2-phosphoglycerate to phosphoenolpyruvate. Kinetic characterisation of enolase was carried out by fitting a reversible Michaelis-Menten rate equation (Eq. 4.9) to the kinetic data. This allowed for the maximal forward specific activity and binding coefficient ($K_{2\text{-PG}}$) of enolase to be determined, however the reverse kinetics of enolase could not be measured. In Fig. 4.9 we display the fitted hyperbolic curve and kinetic data, and the parameters obtained from the fit is shown in Table 4.9.

$$vENO = \frac{\mathrm{Vmf} \cdot \frac{\mathrm{p2g}}{\mathrm{Kp2g}} \cdot \left(1 - \frac{\mathrm{pep}}{\mathrm{Keq \cdot p2g}}\right)}{\frac{\mathrm{p2g}}{\mathrm{Kp2g}} + \frac{\mathrm{pep}}{\mathrm{Kpep}} + 1} \tag{4.9}$$

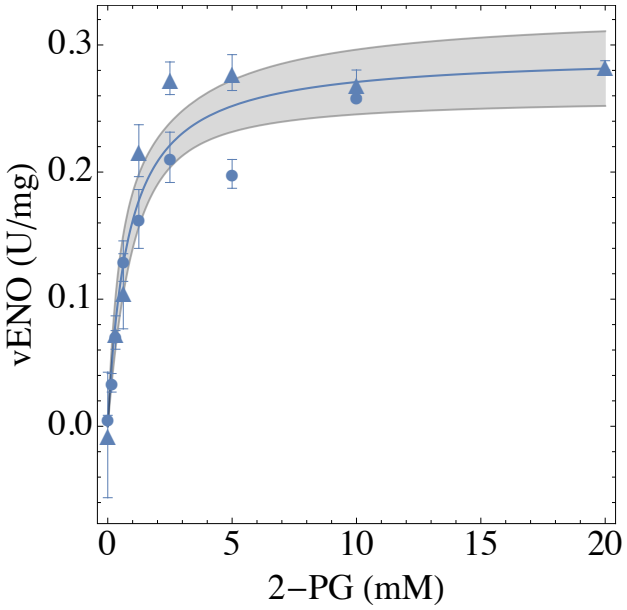

Figure 4.9: Kinetic characterisation of enolase in MDA-mb-231 cells. The maximal specific forward activity and substrate affinity was calculated via fitting the Michaelis-Menten rate equation (Eq. 4.9) to the kinetic data. The symbols (disc and triangle) indicate the two independent experiments. The fit is shown with a 95% confidence prediction interval (grey region) and the error bars are SD of the technical triplicates.

Table 4.9: Overview of kinetic parameters for enolase in MDA-mb-231 cells. The forward maximal specific activity and substrate affinity was determined by fitting the rate equation (Eq. 4.9) to the experimental data. The determined parameters are listed below with values given as mean ± SE.

Parameter	Fitted Value	Literature Value	References
$V_{f\,ENO}$(μmol.min^{-1}.mg^{-1} protein)	0.29 ± 0.016	0.36[1]	[8]
$K_{2\text{-}PG}$(mM)	0.81 ± 0.17	0.038[1]	[8]
K_{PEP}(mM)	-	0.06[1]	[8]
K_{eq}(mM)	-	6.7	[9]

[1]Determined in HeLa cells

4.1.10 Pyruvate Kinase

Pyruvate kinase catalyses the dephosphorylation of phosphoenolpyruvate to pyruvate with the concomitant phosphorylation of ADP to ATP. The maximal specific activity, substrate and product binding coefficients of PK were characterised. Saturation curves shown in Fig. 4.10, demonstrated PEP inhibition at concentrations above 5 mM, however, the sensitivity to PEP inhibition is shown to be dependent on concentration of ADP present. Product inhibition by ATP was observed, whereas PK was insensitive to pyruvate (pyruvate at 10 mM had no effect), data not shown. Characterisation of the kinetic data was achieved by fitting a random-order bi-substrate irreversible Michaelis-Menten equation (Eq. 4.10), with substrate inhibition to the kinetic data. The parameter values obtained are listed in Table 4.10.

$$vPK = \frac{\mathrm{Vmf} \cdot \frac{\mathrm{adp \cdot pep}}{\mathrm{Kadp \cdot Kpep}}}{(1 + \frac{\mathrm{adp}}{\mathrm{Kadp}} + \frac{\mathrm{atp}}{\mathrm{Kiatp}}) \cdot (1 + \frac{\mathrm{pep}}{\mathrm{Kpep}}) \cdot (1 + \frac{\mathrm{pep}}{\mathrm{Kipep}} + \frac{\mathrm{pep}^2}{\mathrm{Kipep}^2})} \tag{4.10}$$

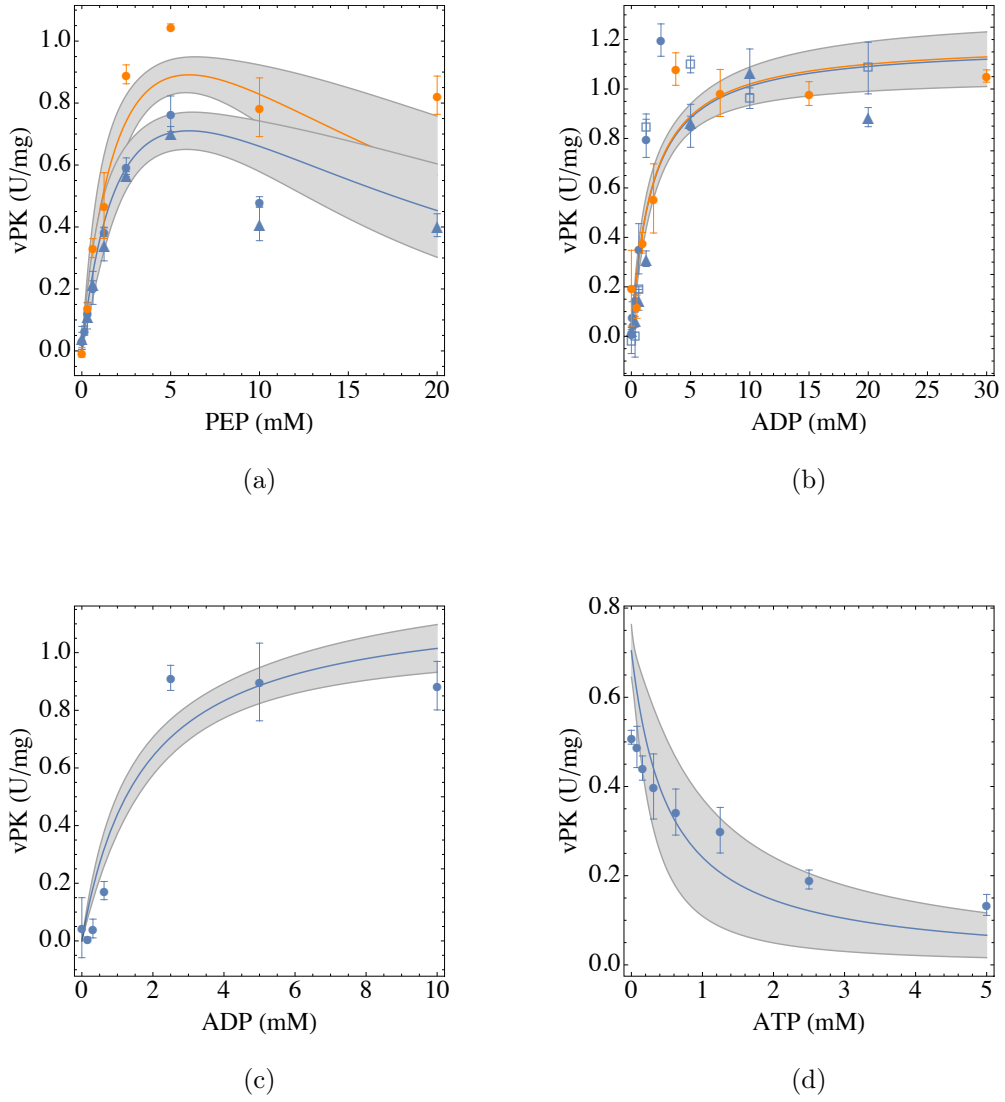

Figure 4.10: Kinetic characterisation of pyruvate kinase in MDA-mb-231 cells. Parameters were obtained by fitting the Michaelis-Menten rate equation (Eq. 4.10) to the kinetic data. Each panel and symbol (disk, triangle and square) represents an independent experiment. The fitted curves shown are depicted with 95% confidence prediction interval bands (grey region). The 95% confidence prediction interval was only included for different conditions within a panel when the fits did not follow the same trend, as seen in panel (a). The PK assay in panel (a) was performed by varying PEP concentrations at 2.5 mM (blue) and 5 mM (orange) ADP; (b) by varying ADP concentrations at 5 mM (blue) and 5.7 mM (orange) PEP and 7 mM PEP in panel (c), ATP inhibition (d) was determined at 5 mM PEP and 2.5 mM ADP. Error bars are SD of the technical triplicates.

Table 4.10: Overview of kinetic parameters for pyruvate kinase in MDA-mb-231 cells. The rate equation (Eq. 4.10) fitted to the experimental kinetic data in order to determine the forward specific activity and affinity constants for PEP, ADP and ATP. Parameters are shown as mean ± SE.

Parameter	Fitted Value	Literature Value	References
$V_{f\,PK}$(μmol.min^{-1}.mg^{-1} protein)	2.3 ± 0.61	5.4 ± 0.16	[48]
K_{PEP}(mM)	2.7 ± 1.3	0.014[2]	[8]
K_{ADP}(mM)	1.7 ± 0.31	0.4[2]	[8]
$K_{i\ ATP}$(mM)	0.21 ± 0.097	-	-
$K_{i\ PEP}$(mM)	22 ± 8.7	-	-

[1]Determined in Bcap37 breast cancer cells
[2]Affinity constants were measured in HeLa cells

F16BP induced no allosteric feed-forward activating effect on PK - data not shown - suggesting that the PKM2 is not the dominant isoform expressed in MBA-mb-231 or that the F16BP concentration in the cell extract is adequate to activate PKM2 in the assay conducted [33, 46].

4.1.11 Lactate Dehydrogenase

Lactate dehydrogenase catalyses the reversible conversion of pyruvate to lactate via oxidation of NADH to NAD^+. The forward and reverse maximal specific activity, including the binding coefficients (K_{PYR}, $K_{i\,PYR}$, K_{NADH}, K_{LAC} and K_{NAD^+}) of LDH were characterised. Fitted a reversible bi-substrate bi-product Michaelis-Menten rate equation (Eq. 4.11) to the kinetic data for LDH in MDA-mb-231 breast cancer cells to obtain the kinetic parameters in Table 4.11. In addition, pyruvate inhibition was observed at concentrations above 5 mM and therefore pyruvate substrate inhibition was added to the rate equation. NADH saturation curves proved difficult to obtain experimentally and according to the rate equation's fitted curve (in Fig. 4.11), NAD^+ is yet to reach saturation. Although the data are quite well described by the rate equation, from the very large error values seen in Table 4.11, it is clear that the parametrisation was problematic, and a more complete dataset is required for a better estimation of the parameter values.

$$vLDH = \frac{\mathrm{Vmf} \cdot \frac{\mathrm{nadh \cdot pyr}}{\mathrm{Knadh \cdot Kpyr}} - \mathrm{Vmr} \cdot \frac{\mathrm{lac \cdot nad}}{\mathrm{Klac \cdot Knad}}}{\left(\frac{\mathrm{pyr}}{\mathrm{Kipyr}} + 1\right)\left(\frac{\mathrm{lac}}{\mathrm{Klac}} + \frac{\mathrm{pyr}}{\mathrm{Kpyr}} + 1\right)\left(\frac{\mathrm{nad}}{\mathrm{Knad}} + \frac{\mathrm{nadh}}{\mathrm{Knadh}} + 1\right)} \tag{4.11}$$

Table 4.11: Overview of kinetic parameters for lactate dehydrogenase in MDA-mb-231 cells. The maximal specific activities and binding affinities were characterised by fitting the rate equation (Eq. 4.11) to the experimentally obtained kinetic data. Values are given as mean ± SE.

Parameter	Fitted Value	Literature Value	References
$V_{f\,LDH}$(μmol.min^{-1}.mg^{-1} protein)	$13 \pm 1.2 \times 10^7$	1.9 ± 0.15[1]	[48]
$V_{r\,LDH}$(μmol.min^{-1}.mg^{-1} protein)	2.9 ± 39	-	-
K_{PYR}(mM)	$2.5 \pm 2.2 \times 10^6$	0.3[2]	[8]
$K_{i\,PYR}$(mM)	$2.5 \pm 2.2 \times 10^6$	-	-
K_{NADH}(mM)	0.42 ± 0.17	-	-
K_{LAC}(mM)	8.6 ± 16	-	-
K_{NAD^+}(mM)	6.3 ± 96	-	-

[1]Determined in Bcap37 breast cancer cells
[2]Affinity constant was measured n HeLa cells

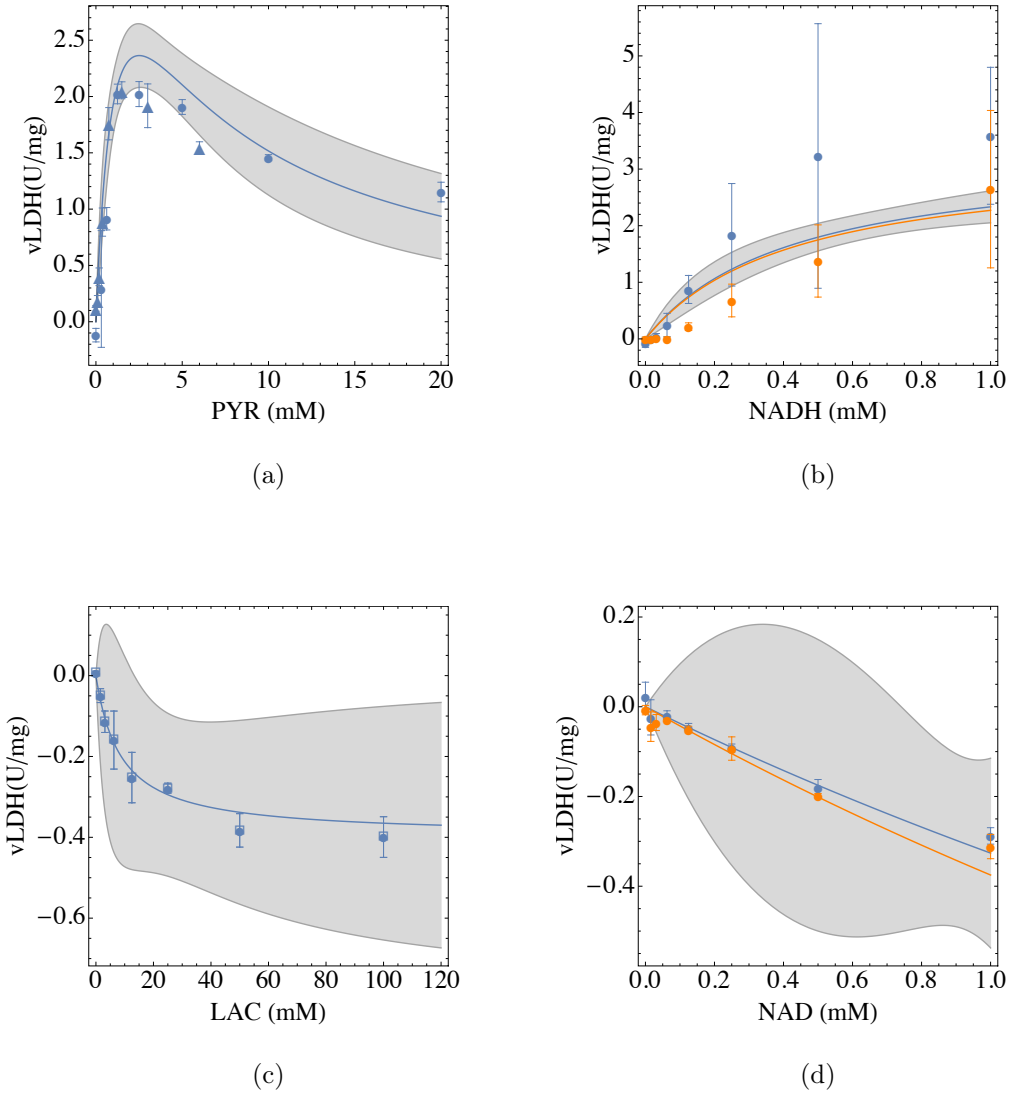

Figure 4.11: Kinetic characterisation of lactate dehydrogenase in MDA-mb-231. Each panel and symbol (disc, triangle and square) is an independent experiment. The blue and orange curve correspond with the kinetic data of the same colour, which were obtained under different conditions. Fitted curves are shown with a 95% confidence prediction interval with the exception of panel (b) and (d) as the confidence prediction interval follow the same trend for both conditions. The LDH assay was performed in panel (a) by varying PYR at 1 mM NADH; in panel (b) by varying NADH concentrations at 2 mM (blue) and 3.75 mM (orange) PYR. The LDH reverse reaction was assayed by varying LAC in panel (c) at 1 mM NAD^+; by varying NAD^+ in panel (d) at 40 mM (blue) and 150 mM (orange) LAC. Error bars represent SD of the technical triplicates.

4.1.12 Adenylate Kinase

Adenylate kinase catalyses interconversion of ADP to ATP and AMP. The maximal specific activities and substrate binding coefficients (K_{ADP}, K_{ATP} and K_{AMP}) of AK were characterised. Results display a typical hyperbolic saturation curve for both reaction directions with the maximal reverse specific activity being greater, as shown in Fig. 4.12. The upper and lower limits of the reverse specific activity were determined via the Haldane relation. Fitted a rate equation (Eq. 4.12) to the kinetic data to obtain the parameters listed below in Table 4.12.

$$v\mathrm{AK} = \frac{\mathrm{Vmf}\cdot\frac{\mathrm{adp}^2}{\mathrm{Kadp}^2}\cdot\left(1-\frac{\Gamma}{\mathrm{Keq}}\right)}{1+\frac{\mathrm{adp}}{\mathrm{Kadp}}\cdot\left(2+\frac{\mathrm{adp}}{\mathrm{Kadp}}+2\,\frac{\mathrm{amp}}{\mathrm{Kamp}}\right)+\frac{\mathrm{amp}}{\mathrm{Kamp}}\cdot\left(2+\frac{\mathrm{amp}}{\mathrm{Kamp}}+\frac{\mathrm{atp}}{\mathrm{Katp}}\right)+\frac{\mathrm{atp}}{\mathrm{Katp}}} \tag{4.12}$$

Table 4.12: Overview of kinetic parameters for adenylate kinase in MDA-mb-231 cells. Fitted the random-ordered Michaelis-Menten equation (Eq. 4.12) to the AK kinetic data to characterise maximal specific activities and binding affinities to obtain the parameters listed below. Values shown as mean ± SE.

Parameter	Fitted Value	Literature Value	References
$V_{f\ AK}$(μmol.min^{-1}.mg^{-1} protein)	0.080 ± 0.010	-	-
$V_{r\ AK}$(μmol.min^{-1}.mg^{-1} protein)	0.12 - 0.22	-	-
K_{ADP}(mM)	0.023 ± 0.011	-	-
K_{ATP}(mM)	0.0049 ± 0.0031	-	-
K_{AMP}(mM)	0.11 ± 0.046	-	-
K_{eq}(mM)	-	0.45	[9]

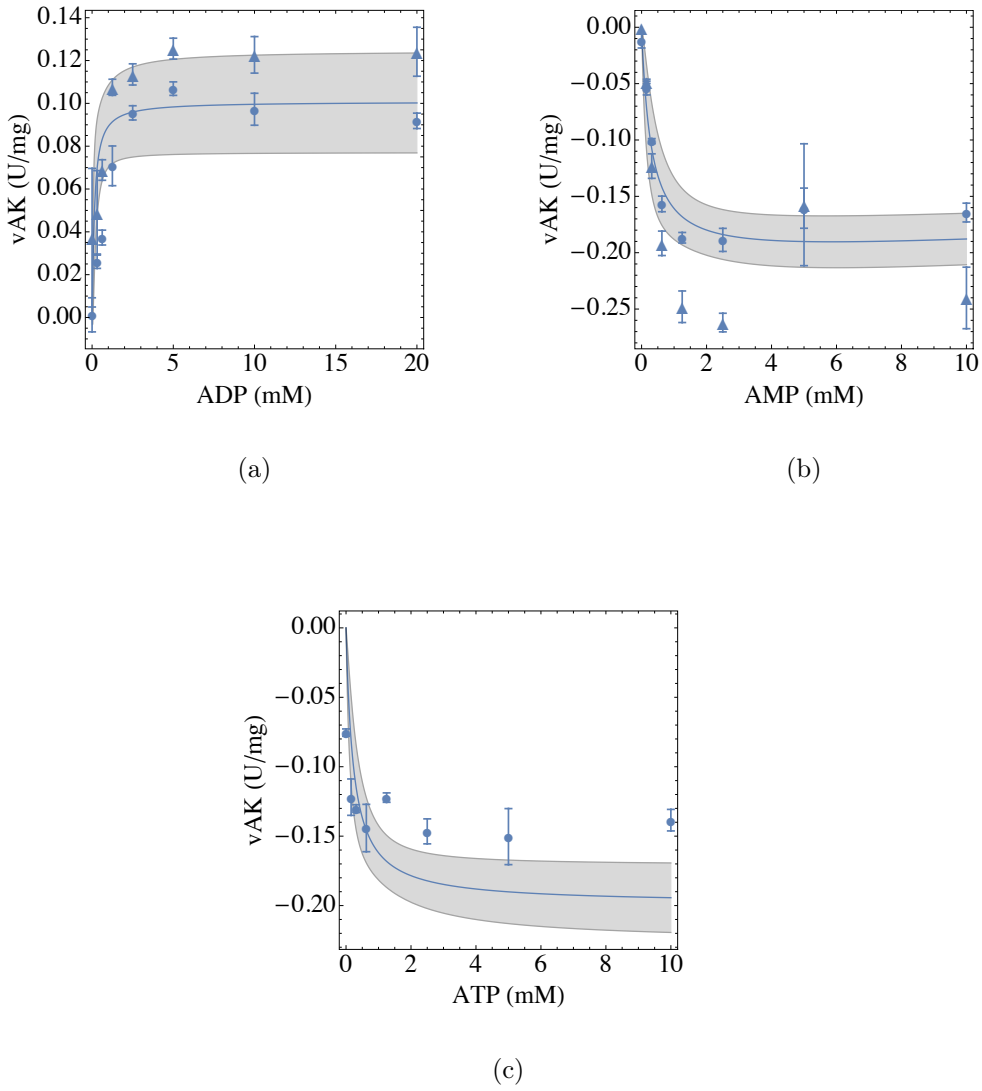

(a) (b)

(c)

Figure 4.12: Kinetic characterisation of adenylate kinase in MDA-mb-231. The forward and reverse maximal specific activity and affinity constants were characterised by fitting the rate equation (Eq. 4.12) to the kinetic data. Each panel and symbol shown represents an independent experiment. The fitted curves are shown with 95% confidence prediction intervals (grey region). Reverse reaction assays varying ATP and AMP in panels (b) and (c), were performed at 5 mM AMP and 5 mM ATP, respectively. The data points are shown as mean SD of the technical triplicates.

4.2 Model Construction

4.2.1 Parameters and Ordinary differential equations

A detailed kinetic model for glycolysis in MDA-mb-231 cells, which describes dynamics of glycolytic intermediates *in vitro* was constructed. Ordinary differential equations (ODEs) were used to represent this dynamic biological system. This mathematical approach could be employed as the mechanisms of glycolysis are known and one can assume that the distribution of molecules is homogenous within a cell extract. This mathematical model was constructed by integrating all parameter values and rate equations into ODEs to predict the change in glycolytic intermediates over time. In addition, the ATPase reaction (Eq. 4.13) was included in the model, where the parameter for this reaction was taken from an in-house glycolysis model for differentiated C_2C_{12} cells [64]. This is a mouse skeletal muscle cell line, which we used for the model construction due to the absence of ATPase kinetic data (obtained at physiological conditions) in human tissue to date in the literature.

$$vATPase = VfATPase \cdot ATP \tag{4.13}$$

The specific activity in the rate equations used to characterise the glycolytic enzymes was expressed as μmol.min^{-1}.mg^{-1} total protein, which was converted to mM.min^{-1} for the simulation. This was achieved by multiplying and dividing the specific activity by the total protein (mg/mL) and volume (mL), respectively. Total protein and volume were obtained from the MDA-mb-231 cell extract used in the metabolomic analysis experiment.

The glycolytic model constructed for MDA-mb-231 cells consists of 17 ODEs (Eq. 4.14– 4.30) that describe the change of intermediate concentrations as a function of time and the rate of glycolytic enzymes, as shown below. The following indicate the rates of glycolytic enzymes: vHK (Hexokinase, Eq. 4.1), vPGI (Phosphoglucoisomerase, Eq. 4.2), vPFK (Phosphofructokinase, Eq. 4.3), vALD (Aldolase, Eq. 4.4), vTPI (Triosephosphate isomerase, Eq. 4.5, vGAPDH (Glyceraldehyde 3-phosphate dehydrogenase, Eq. 4.6), vPGK (Phosphoglycerate kinase, Eq. 4.7), vPGM (Phosphoglycerate mutase, Eq. 4.8), vENO (Enolase, Eq. 4.9), vPK (Pyruvate kinase, Eq. 4.10), vLDH (Lactate dehydrogenase, Eq. 4.11), vAK (Adenylate kinase, Eq. 4.12) and vATPase (Eq. 4.13). The corresponding parameter values, affinity constants and specific activities (see Tables 4.13– 4.14) were incorporated into the rate equations.

Table 4.13: An overview of all specific activity parameters for the MDA-mb-231 cancer cell line. Parameter values that could not be experimentally determined were sourced from literature of other cancer cell lines or other applicable cells but are not listed here (see Addendum A.1). The parameter values presented below are mean ± SE.

Maximal forward and reverse specific activity (μmol.min^{-1}.mg^{-1} protein)				
Enzyme	Parameter	Fitted Value	Parameter	Fitted Value
HK	$V_{f\,HK}$	0.057 ± 0.0027	-	-
PGI	$V_{f\,PGI}$	0.22 ± 0.029	$V_{r\,PGI}$	0.55 ± 0.046
PFK	$V_{f\,PFK}$	0.16 ± 0.033	-	-
ALD	$V_{f\,ALD}$	0.056 ± 0.0057	-	-
TPI	-	-	$V_{r\,TPI}$	1.7 ± 0.29
GAPDH	-	-	$V_{r\,GAPDH}$	0.45 ± 0.11
PGK	-	-	$V_{r\,PGK}$	0.55 ± 0.040
PGM	$V_{f\,PGM}$	2.0 ± 0.10	$V_{r\,PGM}$	0.61 ± 0.079
ENO	$V_{f\,ENO}$	0.29 ± 0.016	-	-
PK	$V_{f\,PK}$	2.3 ± 0.61	-	-
LDH	$V_{f\,LDH}$	13 ± 1.2 × 10^7	$V_{r\,LDH}$	2.9 ± 39
AK	$V_{f\,AK}$	0.080 ± 0.010	$V_{r\,AK}$	0.12 - 0.22

$$ATP'[t] = -vHK - vPFK + vPGK + vPK + vAK - vATPase \quad (4.14)$$

$$ADP'[t] = vHK + vPFK - vPGK - vPK - 2.0vAK + vATPase \quad (4.15)$$

$$AMP'[t] = vAK \quad (4.16)$$

$$GLCIn'[t] = -vHK \quad (4.17)$$

$$G6P'[t] = vHKvPGI \quad (4.18)$$

$$F6P'[t] = vPGI - vPFK \quad (4.19)$$

$$F16BP'[t] = vPFK - vALD \quad (4.20)$$

$$DHAP'[t] = vALD - vTPI \quad (4.21)$$

$$GAP'[t] = vALD + vTPI - vGAPDH \quad (4.22)$$

$$B13PG'[t] = vGAPDH - vPGK \quad (4.23)$$

$$NAD'[t] = vGAPDH + vLDH \quad (4.24)$$

$$NADH'[t] = vGAPDH - vLDH \quad (4.25)$$

$$P3G'[t] = vPGK - vPGM \quad (4.26)$$

$$P2G'[t] = vPGM - vENO \quad (4.27)$$

$$PEP'[t] = vENO - vPK \quad (4.28)$$

$$PYRIn'[t] = vPK - vLDH \quad (4.29)$$

$$LACIn'[t] = vLDH \quad (4.30)$$

Table 4.14: An overview of the experimentally determined affinity constants for the MDA-mb-231 cancer cell line. The parameter values acquired from the literature are not shown (see Addendum A.1). Affinity constant parameters shown are mean ± SE.

Substrate and product binding coefficients (mM)				
Enzyme	Parameter	Fitted Value	Parameter	Fitted Value
HK	K_{GLC}	0.096 ± 0.017	K_{ATP}	0.89 ± 0.14
	K_{iADP}	24 ± 8.8	$K_{i\ AMP}$	8.9 ± 2.1
PGI	K_{G6P}	0.32 ± 0.30	K_{F6P}	1.0 ± 0.30
PFK	K_{F6P}	0.52 ± 0.12	K_{ATP}	0.77 ± 0.33
	$K_{i\ ATP}$	9.8 ± 2.9	K_{iADP}	1.2 ± 0.67
	$K_{i\ AMP}$	12 ± 7.7	-	-
ALD	K_{F16BP}	0.41 ± 0.15	-	-
TPI	K_{GAP}	1.2 ± 0.52	-	-
GAPDH	$K_{B1,3PG}$	0.029 ± 0.018	K_{NADH}	0.15 ± 0.13
PGK	$K_{3\text{-}PG}$	1.7 ± 0.42	K_{ATP}	0.32 ± 0.079
PGM	$K_{3\text{-}PG}$	1.0 ± 0.17	$K_{2\text{-}PG}$	0.82 ± 0.41
ENO	$K_{2\text{-}PG}$	0.81 ± 0.17	-	-
PK	K_{PEP}	2.7 ± 1.3	K_{ADP}	1.7 ± 0.31
	$K_{i\ ATP}$	0.21 ± 0.097	$K_{i\ PEP}$	22 ± 8.7
LDH	K_{PYR}	$2.5 \pm 2.2 \times 10^6$	$K_{i\ PYR}$	$2.5 \pm 2.2 \times 10^6$
	K_{NADH}	0.42 ± 0.17	K_{LAC}	8.7 ± 16
	K_{NAD^+}	6.3 ± 96	-	-
AK	K_{ADP}	0.023 ± 0.011	K_{ATP}	0.0049 ± 0.0031
	K_{AMP}	0.11 ± 0.046	-	-

4.3 Conclusion

In this chapter a detailed mathematical model for glycolysis in the breast cancer cell line MDA-mb-231 was constructed. For this, we characterised all the glycolytic enzymes under physiological conditions, in *in vitro* kinetic assays. Although most of the kinetic constants could be fitted on the experimental data, we had to use some literature values for some of the parameters. In the next chapter we will validate the model.

Chapter 5

Results and Discussion: Glycolytic Model Validation

In this chapter, we analyse and compare the experimental data to the mathematical model that was constructed in Chapter 4, to validate the model. We measured the glucose to lactate flux enzymatically and conducted a ^{14}C-glucose metabolomic time-course experiment to investigate the time-dynamics of glycolytic intermediates. We subsequently, employed the model to simulate the above-mentioned experiments. The glycolytic flux in MDA-mb-231 was also compared to a non-invasive MCF-7 breast cancer cell line and the effect of insulin on the glycolytic flux in both cell lines was determined.

5.1 Enzymatic glycolytic flux analysis

We measured the flux through glycolysis in intact cells by determining glucose consumption and lactate production extracellularly. This experiment was conducted over a period of 9 hours to reduce the potential for cell growth to skew results. The results indicate that MDA-mb-231 has a greater flux than MCF-7, as can be seen in Fig. 5.1 and Table 5.1. The glycolytic efficiency was approximately 1.7 moles of lactate generated per glucose consumed for both cell lines. These results are similar to published values: MCF-7 and MDA-mb-231 have been reported to generate 1.5 and 1.8 moles of lactate per glucose, respectively [63].

The effect of insulin on glycolysis showed a slight increase in uptake, yet production marginally decreased glycolytic efficiency (1.6 and 1.5 in MDA-mb-231 and MCF-7 cells, respectively). This correlates with what is described in the literature as glucose uptake in cancer cells tend to occur independent of insulin simulation [37]. This experiment provided an estimation of glucose to lactate conversion in MDA-mb-231 cells and how it compares to the MCF-7 cancer cell line.

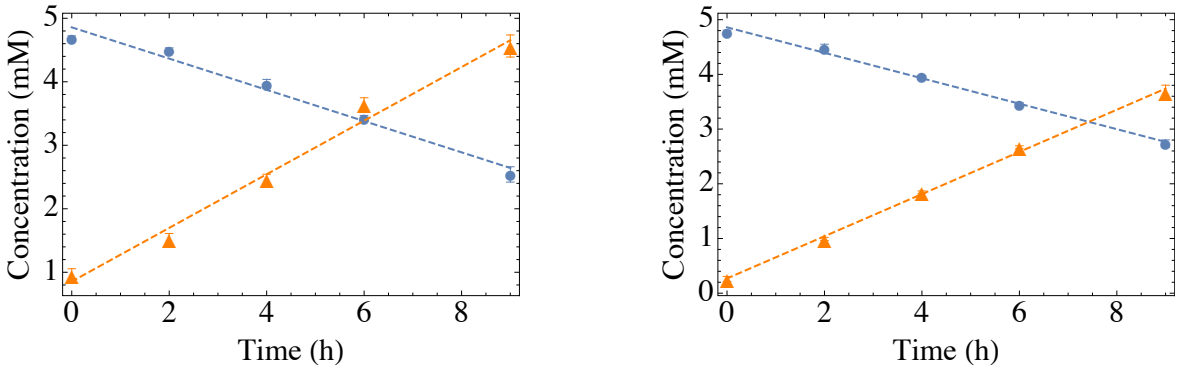

(a) (b)

Figure 5.1: The time-dependent consumption of glucose (blue, disc) and production of lactate (orange, triangle), in both MDA-mb-231 (a) and MCF-7 (b) cells. The extracellular change in glucose and lactate concentrations was measured over 9 hours via enzymatic glucose and lactate determination assays. Flux data was normalised to protein concentration and error bars depict SEM of three independent experiments.

Table 5.1: The glucose consumption and lactate production rates in MDA-mb-231 cells and MCF-7 breast cancer cell lines. Values given represent the mean ± SEM of three independent experiments. Consumption rates are given as negative values.

Cell line	MDA-mb-231	MCF-7
Metabolites	Flux ($nmol.min^{-1}.mg^{-1}protein$)	
D-Glucose	-52 ± 2.5	-23 ± 0.18
L-Lactate	89 ± 7.4	38 ± 1.26

The MDA-mb-231 cell line is more dependent on glycolysis to meet its bioenergy demands than the MCF-7 cells. Lunetti *et al.* [14] provided evidence for this difference, showing that the mitochondria in MDA-mb-231 cells

were highly dysfunctional when compared to the MCF-7 cells, which allows the latter to generate ATP via oxidative phosphorylation, therefore making them less reliant on glycolysis. However, the comparable glucose to lactate ratio indicates that the difference in fermentative to oxidative metabolism is not dramatic. It should also be noted that the MDA-mb-231 cell line exhibits a slightly higher exponential growth rate compared to the MCF-7 [53, 63]. The higher rate of ATP production could be advantageous for the rapid proliferation of MDA-mb-231 cells.

5.2 Model analysis and validation

We constructed a detailed mathematical model that describes the dynamics of glycolysis, to predict the change of variables within the pathway. To achieve this, we combined the parameter values and rate equations, as obtained in Chapter 4, into ODEs that describe the evolution in time of the glycolytic intermediates within the MDA-mb-231 cell extract.

We compared simulation output to experimental data obtained from ^{14}C-glucose labelled time-course experiments. Using ^{14}C-glucose isotope allowed us to trace the glycolytic flux within cell extract. The cell extract was incubated at 37°C in assay buffer and subsequently, the time-course experiment was initialised by the addition of ATP, NAD^+ and ^{14}C-GLC (including unlabelled glucose), as described in Section 3.7. Time-course samples were collected, starting from 0'. The samples were analysed by using an in-house ion-pairing reverse HPLC (IP-RPLC) method to separate glycolytic intermediates within the cell extract.

UV-Vis and radiolabelled detectors were used to quantify co-factors and ^{14}C-glycolytic intermediates, respectively, as described in Section 3.7. The UV-Vis detector provided the peak area count of adenosine and nicotinamide from which we determined the co-factor concentration using a standard curve. In comparison, the radiolabelled detector generated a chromatographic trace for each sample and effectively traced metabolites through glycolysis to lactate via the ^{14}C-carbon signal. By employing an in-house written Wolfram Mathematica script, we were able to quantify the peak area count for the metabolites present and the concentration was determined from the response factor calculated using the initial ^{14}C-glucose introduced. We conducted time-course experiments with and without 2,3-BPG (in duplicate) during the incubation step. The reason for these two sets of experiments was as a result of the deviation we observed between the model simulation and validation experiment, which led us to PGM and its influence on glycolysis (as shown in Section 4.1.8), which will be discussed in this section.

The model simulated the experimental conditions by using the initial chromatographic results obtained (sample 0') as the initial state of the system to be simulated. The initial values, shown in Table 5.2, were taken as the mean

of initial concentrations determined in the duplicate experiments. The total protein measured were 5.0 and 4.9 mg protein in the experiments with and without added 2,3-BPG, respectively, and the total volume was 1 mL in both sets of experiments. For both set of experiments we were able to recover the vast majority (93% ± 3.6) of the carbon introduced to the cell extract. In this section we will, discuss the comparison between the model simulation and validation data.

Table 5.2: The initial metabolite concentrations used in the model simulating low PGM activity and 2,3-BPG bound PGM in the time-course experiment where 2,3-BPG was absent and added, respectively. These values are the mean concentrations of metabolites detected at 0 min of the time-course experiment.

Model simulation	Low PGM activity (Fig. 5.2)	Activated PGM (Fig. 5.3)
Metabolite (mM)	Initial Value	
GLC	1.0	1.0
G6P	0.030	0.045
F6P	0.051	0.015
F16BP	0.0	0.0091
LAC	0.17	0.0
NAD^+	0.88	1.0
NADH	0.0	0.043
ATP	1.1	1.4
ADP	0.27	0.30
AMP	0.28	0.013

5.2.1 Model simulation predicting change in glycolytic metabolites *in vitro* compared to experimental results without the addition of 2,3-BPG.

In the first set of experiments we did not add additional 2,3-BPG, the PGM co-activator. Analysis of the time-course experiment provided chromatographic traces, which provided the time-dynamics of metabolites and co-factors in glycolysis. To determine the accuracy of the model simulating the glucose to lactate conversion in a cell extract. We compared the model prediction to the validation data obtained, shown in Fig. 5.2.

Two parameters that were taken from the literature, as described in Chapter 4, were changed in order to make the model simulations. These alterations are the parameter values of $V_{f\,ATPase}$ and $V_{f\,GAPDH}$, which were both decreased. The parameter value of $V_{f\,GAPDH}$ was far too great compared to the $V_{r\,GAPDH}$ when considering K_{eq}. Hence, we decided to fit the $V_{f\,GAPDH}$ parameter, despite that, in theory, one could determine the forward specific activity from the Haldane equation. However, to achieve this would be a difficult feat due to the precariousness of K_{B13PG}.

In addition, we modified the initial value of ADP to a negligible value, i.e. ADP = 0, to further improve the fit and adequately conserve the adenosine moiety. In the absence of 2,3-BPG, PGM activity decreases substantially (presented in the Appendix A.1) and to account for this in the validation experiment, we assumed that the concentration of 2,3-BPG is insufficient, leading to limited PGM activity. As a result, we decreased the specific activity of PGM to give the best description of the experimental data. For it was not possible to measure PGM activity experimentally as the characterisation experiments were performed at a lower protein concentration and therefore lower intrinsic 2,3-BPG concentration. Taken together, these modifications improved the correlation between the simulation and experimental data.

The simulation of 13 variables generated by the model, were compared to the experimental data obtained, as shown in Fig. 5.2. The comparison demonstrated a satisfactory prediction for GLC, G6P, DHAP, 3-PG and LAC. But due to reduced activity of PGM the model simulations showed an under-prediction of 2-PG. It should also be noted that 2-PG formation was only observed in one biological repeat. In the case of adenosine species, only ADP correlated well with the model, whereas the prediction of ATP and AMP showed in a similar trend to the values obtained experimentally, but the model underestimated ATP and overestimated AMP. Similarly, the model exaggerated F6P and F16BP, but the trend predicted by the model was correct.

The model overestimation of F16BP is likely due to underestimated aldolase activity determined in the enzyme assays. The measured forward specific activity of aldolase ($V_{f\,ALD}$) in chapter 4 was almost 4-fold lower compared to aldose activity in Bcap37 and HeLa cells (both measured at 0.2

μmol.min^{-1}.mg^{-1}cytosolic protein) [8, 48]. The overestimation of F6P, by contrast, could be as a result of PFK activity being underestimated. This could be potentially corrected by fitting the kinetics of PFK using a MWC rate equation, which could improve the estimated parameter values of PFK.

The partial glucose to lactate conversion is adequately predicted by the model. LAC is sufficiently produced in the experimental results, albeit at low concentrations (glycolytic efficiency of roughly 0.3 – 0.4). This was accurately predicted by the model, regardless of the decreased PGM activity. However, the rate of LAC production with the concomitant regeneration of NAD^+ was not sufficiently fast in the model. This results in a deviation in the experimental results and model prediction for nicotinamide species.

The predicted 3-PG accumulation is due to reduced PGM activity but mechanisms involved in DHAP accumulation ($\geq$1.0 mM) remains partially unclear. We speculate that TPI activity is underestimated by the rate equation fitted to the kinetic data. In addition, DHAP eludes from the HPLC column at a position where several other metabolites elude, making it difficult to estimate the exact concentration. The experimental data for GAP, B13PG, PEP and PYR could not be quantified. The model simulation for these variables did not exceed concentrations greater than 0.025 mM.

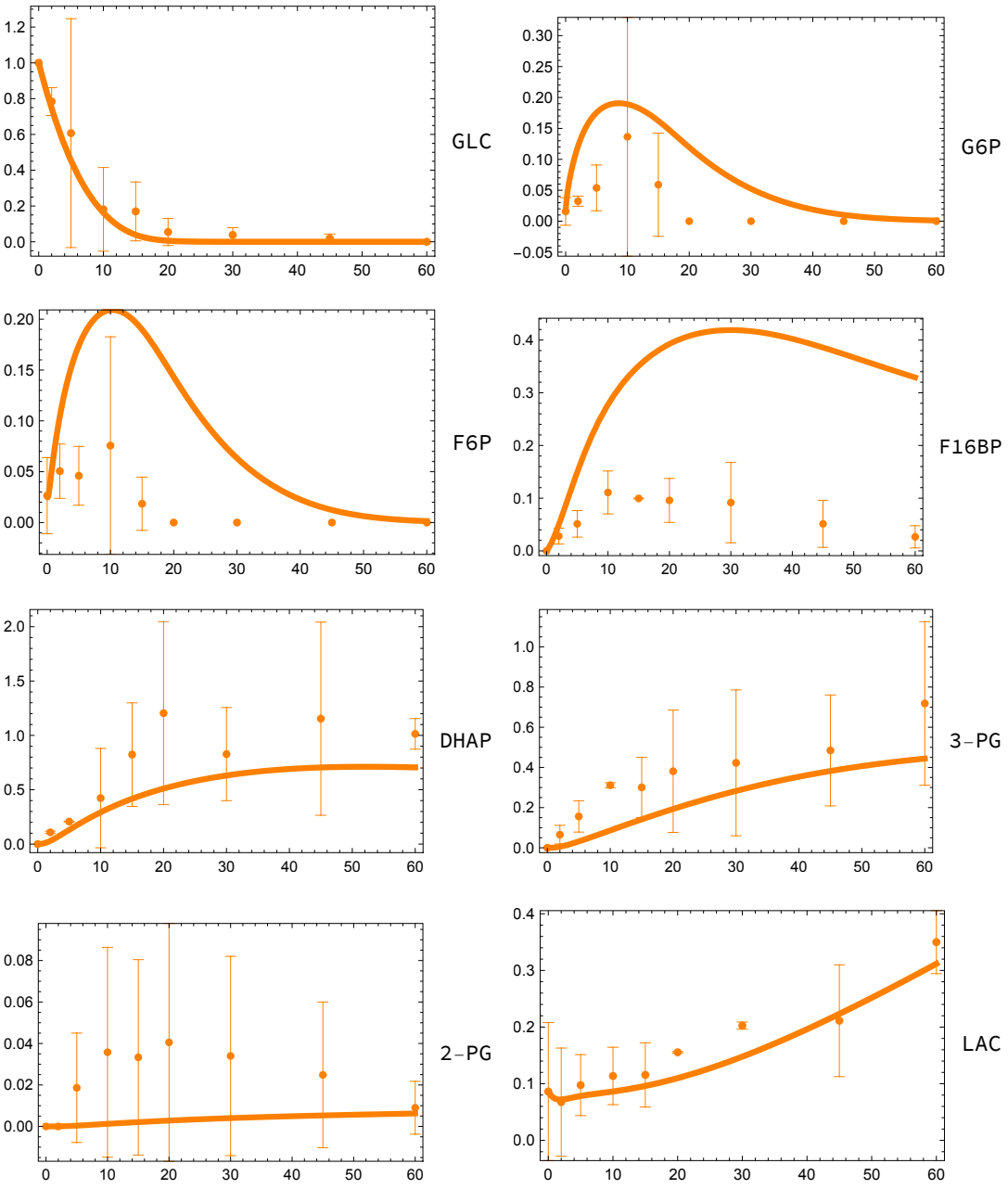

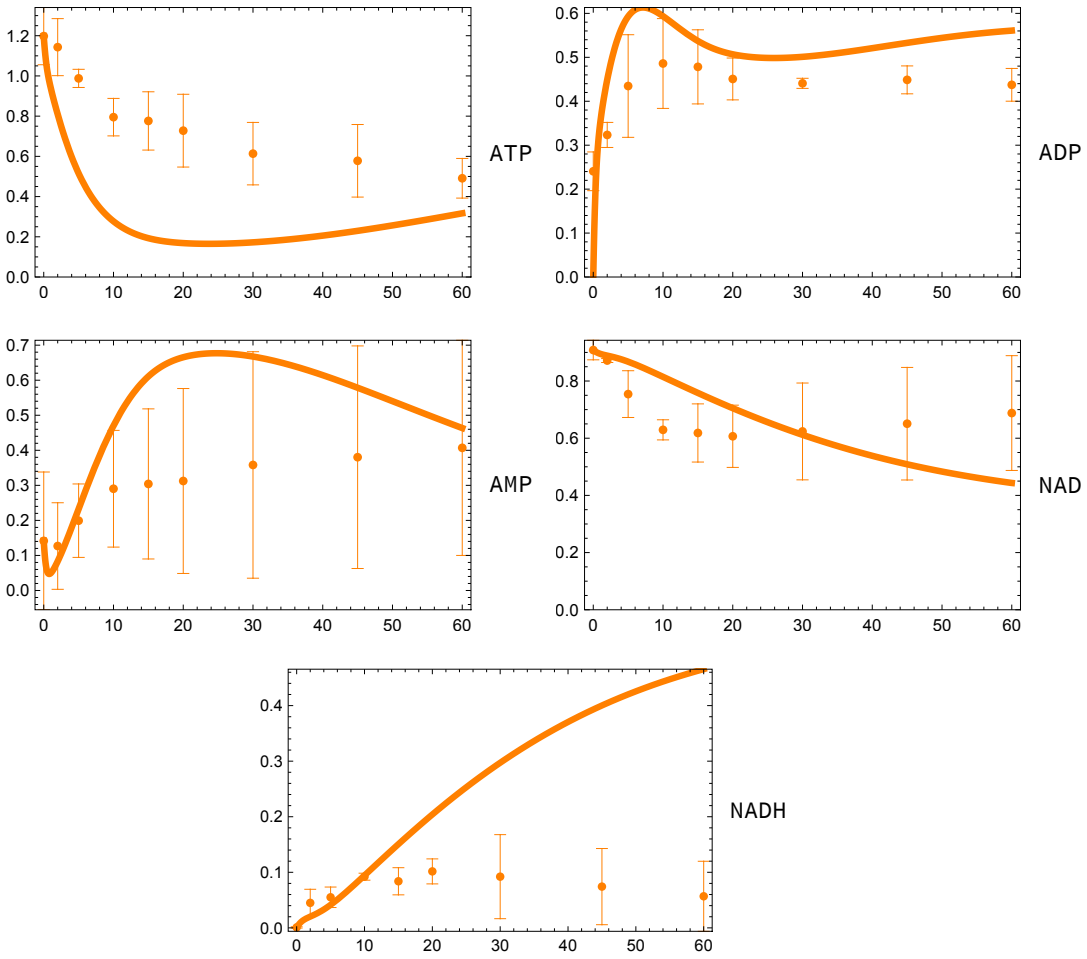

Figure 5.2: Model simulation for glycolytic intermediates compared to experimental results for glucose conversion in MDA-mb-231 cell extract, without added 2,3-BPG. Panels show the simulation (orange curve) and validation data (orange disc), which illustrates the change in metabolite concentration as a function of time over 60 min (x-axis, min; y-axis, mM). Initial values for the model simulation, obtained from the time-sample (0 min) in labelled metabolomic analysis experiment, values listed in Table 5.2. Error bars shown as SD of the biological duplicates.

5.2.2 Model simulation predicting change in glycolytic metabolites *in vitro* compared to experimental results with the addition of 2,3-BPG to the cell extract.

In the second set of experiments we added additional 2,3-BPG, the PGM co-activator. Analysis of the time-course experiment generated chromatographic traces, which provided the time-dynamics of metabolites and co-factors in glycolysis. We determined the model's accuracy in predicting glucose to lactate conversion in MDA-mb-231 cell extract by comparing the model to experimentally obtained results, presented in Fig. 5.3. We could not quantify the experimental results of GAP, B13PG, PEP and PYR. The concentrations of these metabolites did not exceed 0.040 mM in the model prediction.

Two parameters that were taken from the literature, as described in Chapter 4, were also changed in order to make the model simulations. We modified $V_{f\,ATPase}$ and $V_{f\,GAPDH}$ parameter values, where both parameters were decreased. PGM is presumed to function sufficiently in the cell extract when adding 2.0 mM of 2,3-BPG and therefore, no modification of the PGM parameters is required.

We compared the simulation of 13 variables to the experimental data obtained. The simulation and experimental data resulted in a satisfactory correlation for GLC, DHAP, 2-PG and LAC. Adenosine moiety trends were reasonably predicted for ATP and AMP until glucose depletion at 10 min in the experimental data and, hereafter the model under- and overestimated ATP and AMP, respectively. The model could adequately describe the ADP trend observed.

Experimental results for G6P and F6P appeared to correlate relatively well with the model prediction. However, the model overestimated F16BP, predicting its accumulation in the cell extract. In addition, a deviation is observed between the model simulation and experiment results for 3-PG. The model did not reflect this build-up, suggesting that some 3-PG accumulation occurs regardless of the 2,3-BPG activated PGM. Nevertheless, the 3-PG accumulation observed, is 2-fold lower in comparison to the first set of experiments (Fig. 5.2).

To reiterate, 2,3-BPG activated PGM facilitated greater glucose to lactate conversion, which the model was able to predict upon modification. The conversion falls short of what is theoretically possible and observed in the whole-cell flux results in Section 5.1. Glycolytic efficiency in the cell extract is approx. 0.9, whereas extracellular flux results were roughly two-fold greater. This indicates a considerable difference between the whole-cells and cell extract time-dynamics of glycolytic metabolites. The apparent block at DHAP is largely responsible for the low conversion efficiency in the cell extract.

Similarly to the model simulation presented in Fig. 5.2, LDH flux was also

unable to sufficiently regenerate NAD^+. LAC is produced to a greater extent in the current scenario, yet the model still could not predict the dynamic trend of nicotinamide species. The relatively weak description of the GAPDH and LDH obtained in Chapter 4, could be responsible for the contrast between the simulations and experimental results. Hence, more kinetic data for these enzymes could yield improved parameter estimations for K_m and V_{max} values, and thus potentially a better prediction of nicotinamide species.

Both simulation and experimental sets exhibited DHAP accumulation, although DHAP build-up is larger in the low-PGM activity experiment (Fig. 5.2). The DHAP observed, as previously mentioned, might have been exacerbated due to the proximity of DHAP to other peaks in the chromatographic traces. A study conducted on MDA-mb-231 demonstrated the conversion of glucose to glycerol-3 phosphate (G3P) from DHAP for lipid synthesis [53]. In this case, one would observe the consumption of DHAP, leading to a noticeable loss in ^{14}C-carbon in the system as DHAP is shunted towards G3P production. A low flux through glycerol-3 phosphate dehydrogenase (G3PDH) could serve as an explanation for the lack of ^{14}C-carbon redirected due to other chemical species influencing either TPI or G3PDH. Further, as mentioned previously, DHAP accumulation could result in methylglyoxal production, which is a metabolite with anti-cancer properties and consequently detrimental to cancer cells [49]. The extent to which DHAP accumulation occurs in whole-cells remains unclear. Scientific literature has shown HeLa cells to produce a noticeable concentration of DHAP (0.93 ± 0.07 mM) *in vivo* and yet the HeLa TPI (5 μmol.min^{-1}.mg^{-1}cytosolic protein) presents a higher activity compared to the MDA-mb-231 TPI [8].

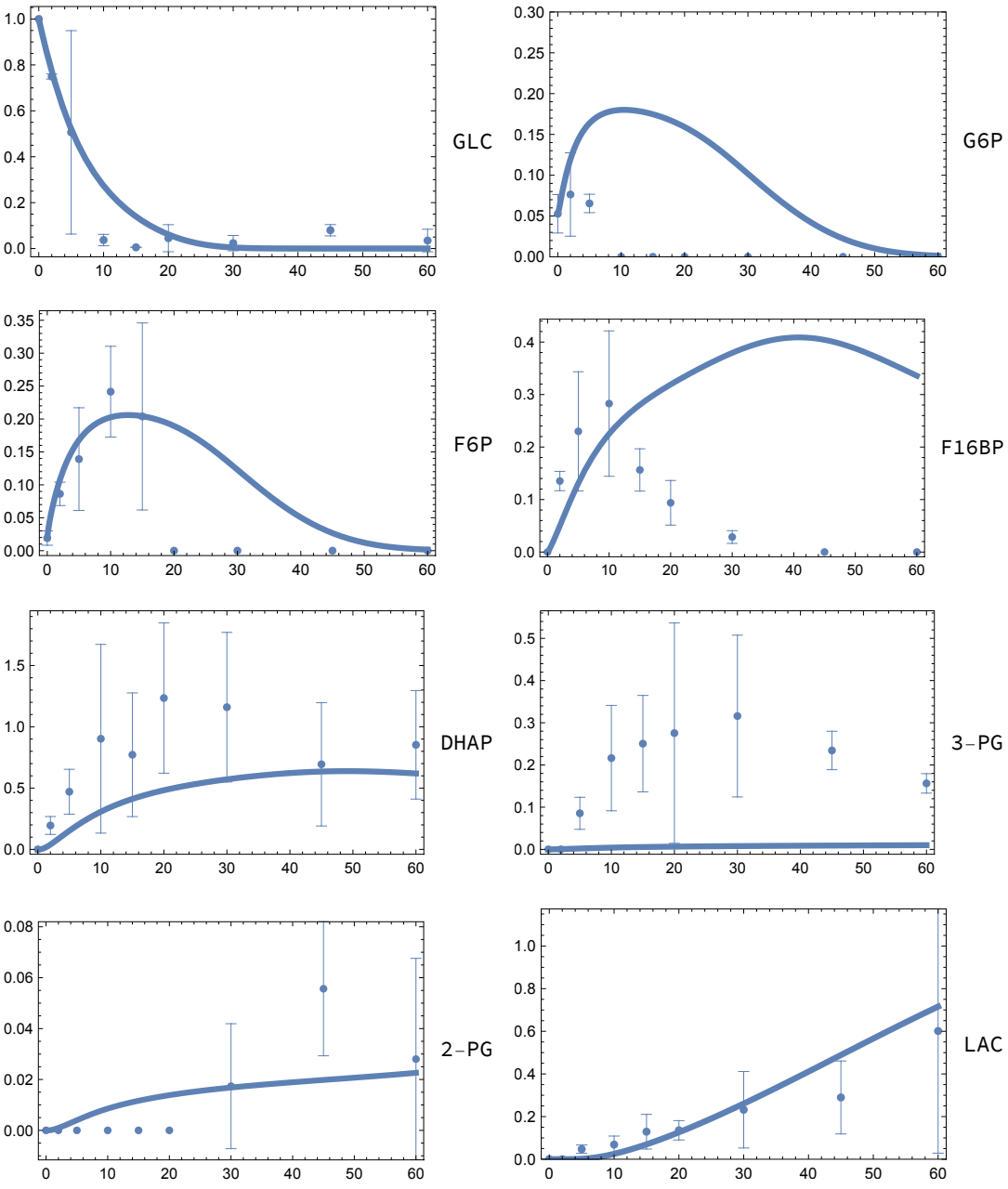

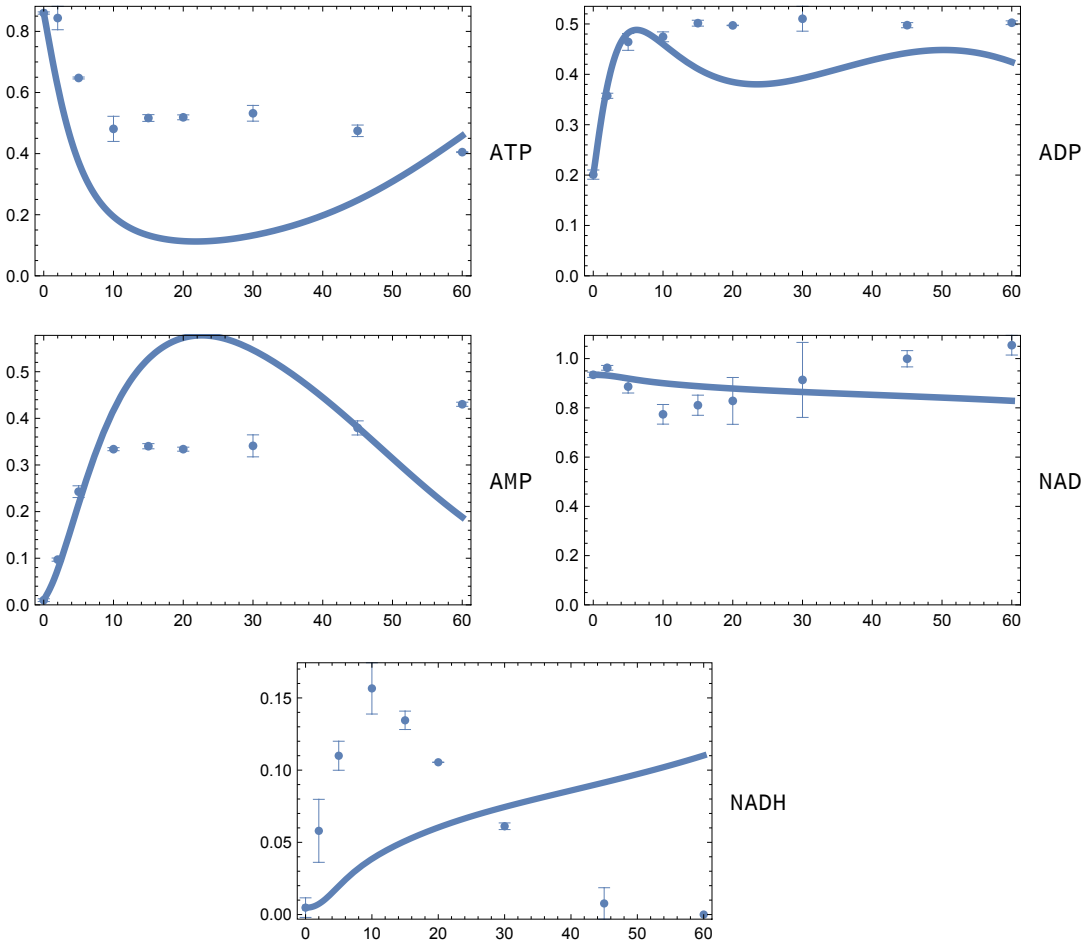

Figure 5.3: Model simulation for glycolytic intermediates compared to experimental results for glucose conversion in MDA-mb-231 cell extract, with added 2,3-BPG. Panels show the simulation (blue curve) and validation data (blue disc) describing the time-dynamics of glycolytic metabolites over 60 min (x-axis, min; y-axis, mM). Initial values for the model simulation, obtained from the time-sample (0 min) in labelled metabolomic analysis experiment, values shown in Table 5.2. Error bars shown as SD of the biological duplicates.

5.3 Conclusion

In this chapter we compared the model simulation to ^{14}C-glucose labelled time-course experiment performed on MDA-mb-231 cell extract, intending to validate the detailed-kinetic model constructed in Chapter 4. However, the accuracy of the model prediction of the experimental data under the two conditions was deemed satisfactory, and therefore partially validated the kinetic model of glycolysis in MDA-mb-231 cell extract. We do acknowledge that this judgement about the model prediction of the experimental data is somewhat subjective.

In addition, we measured the glycolytic flux in MDA-mb-231 whole cells and compared the flux to a less-invasive luminal-like MCF-7 cancer cell line. The glycolytic flux in MDA-mb-231 is 2-fold greater in comparison to the less invasive MCF-7 cells. Interestingly, both cell lines exhibited a similar glucose efficiency, despite the MCF-7 cells being less dependent on glycolysis for its energy demands.

Chapter 6

Concluding remarks

6.1 Conclusion

The metabolic reprogramming in some cancerous cells gives rise to aerobic glycolysis, resulting in cancer cells preferring fermentation of glucose and an enhanced glycolytic flux [2]. Studies have shown that the Warburg effect is due to the dysregulation of oncogenes, the mTOR signalling pathway and the loss of tumour suppressors, among other cellular processes [5, 19, 23, 24]. Literature has suggested that there is a correlation between the invasiveness of cancer cells and their enhanced glycolytic flux [14, 53]. The most frequent cause of death in breast cancer patients diagnosed with TNBC is the tumour metastasising to viscera [13]. Hence, further investigating the association between glycolysis and invasiveness and mobility of cancer cells could be illuminating. The study presented here aimed to determine whether we can explain the glycolytic flux in cancer cells based on its enzyme characteristics. Each of the glycolytic enzymes were characterised in *in vitro* enzyme assays and mechanistic rate equations were fitted to the experimental data. Subsequently, a detailed kinetic model was constructed by combining the parametrised rate equations into ODEs. Finally, we determined the accuracy of model prediction by comparing the simulation to experimental data on the complete pathway.

Classic enzyme kinetic characterisation experiments were conducted under conditions that mimic the cytosolic environment in order to determine physiologically representative parameter values of the enzymes. The enzyme kinetic characterisation results revealed some regulatory mechanisms within the metabolic network. Unexpectedly, aldolase exhibited the lowest activity in the glycolytic pathway. The aldolase activities observed in HeLa, and Bcap37 cells lines were several-fold greater than the activity measured in the MDA-mb-231 cell line [8, 48]. As a result, we would expect a build-up of F16BP in the cell extract, which the time-course experiment confirmed. However, the model overestimated the degree to which F16BP accumulates.

The focus of Chapter 4 was MDA-mb-231 enzyme characterisation and

model construction. The latter involved combining of the parametrised rate equations into 17 ODEs. The ODEs describe changes in the concentration of the variables as a function of time. This bottom-up approach resulted in a detailed-kinetic model that could provide an integrated view of the glycolytic behaviour in MDA-mb-231 cells.

In Chapter 5, we presented the glycolytic flux of MDA-mb-231 whole-cells and compared the flux between invasive basal-like MDA-mb-231 and less-invasive luminal-like MCF-7 cells. The results showed that the glycolytic flux in MDA-mb-231 is roughly 2-fold greater than in the MCF-7 cell line, which correlated with observations in the literature [14, 63].

We simulated the dynamic behaviour of glycolysis in MDA-mb-231 cells *in vitro* and compared it to experimental results to determine the accuracy of the model prediction. This involved performing a tracer-based metabolomic experiment, where we introduced ^{14}C-labelled glucose, ATP and NAD^+ to an incubating MDA-mb-231 cell extract (at 37°C and pH 7.6). Samples during the time-course experiment were collected and analysed using an in-house developed IP-RPLC protocol to quantify the time-dependent change in glycolytic intermediates, adenosine and nicotinamide species. We compared the experimental results to the model simulations to validate the detailed-kinetic model constructed. Two different conditions were simulated: glycolytic dynamics with or without extra added 2,3-BPG (an essential activator of PGM). The model could simulate both conditions with reasonable accuracy, after we adapted two parameters that were taken from the literature. Given the shortcomings with regards to predicting the change in some metabolites, such as the nicotinamide species and F16BP, we conclude that the model is partially validated in these experiments. We could also not compare the experimental data of other metabolites (GAP, PEP and PYR) due to the inability to distinguish them on the chromatograms. Ultimately, the model is robust enough to simulate glycolysis under both *in vitro* conditions. The characteristics of glycolytic enzymes can with reasonable accuracy describe the behaviour of glycolysis in the cell extract. The extracellular glycolytic flux results achieved in the whole-cells is, however, quite different in comparison to the cell extract experimental and model simulation results. In the cell extract glycolysis experiments we could not reproduce the glucose to lactate conversion efficiency observed in the whole-cell experiment.

6.2 Future Studies

The novel detailed-kinetic model developed in this study via the bottom-up approach provides a helpful framework that could be used to further probe glycolysis in highly-invasive breast cancer cells. In addition, the study produced a significant amount of enzyme kinetic data for MDA-mb-231 absent to date in the literature. Further refinement of the model and extrapolation of the

model to simulate a whole-cell would serve as a useful tool to determine the underlying control mechanisms within the pathway and provide a framework to further explore the potential of targeting cancer metabolism for therapeutic strategies.

For future studies it is important to focus on further refinement of the mechanistic model and extrapolating the model to simulate a whole-cell, which should include determining the activity of transporters, e.g. MCT and GLUT. As useful additional validation experiments one could use inhibitor titrations. For instance GAPDH perturbation experiments to determine if the model can predict glycolytic flux subjected to GAPDH inhibition. The mathematical model can be used to probe underlying control mechanisms within the pathway at a steady-state using MCA. This could aid in identifying vulnerable mechanisms within cancer glycolysis that could serve as suitable drug targets.

In a recent publication [29], a network-based selective drug strategy that exploits the difference in control distribution between *T. brucei* and erythrocytes was used, and a similar approach could perhaps be done for tumour cells and healthy cells [29]. Comparing the flux-control steps between MDA-mb-231 and MCF-7 would be an avenue worth exploring, despite their distinct metabolic profiles, to determine whether the flux control distribution in glycolysis is different in highly invasive/metastatic cancer cells compared to less invasive cancer cells [14]. Furthermore, distinct breast cancer cell lines, e.g. MDA-mb-231 and MCF-7, can be studied to quantitatively explore the link between glycolytic flux in breast cancer and, its invasive and malignant properties. This could further lead to identification of potential targets in the glycolysis pathway of invasive cancers for therapeutic treatments and consequently, improve the survival rates of TNBC patients.

Appendices

Appendix A

Enzyme characterisation

A.1 Phosphoglycerate mutase (PGM) kinetics

We determined the degree to which 2,3-BPG effects the co-factor dependent PGM. To do so, coupled enzyme assays at varying concentrations 2,3-PBG were performed whilst initialising the reaction with 10.0 mM 3-PG. The results showed an 18-fold increase in PGM activity when sufficient 2,3-BPG is introduced to the MDA-mb-231 cell extract. This supported our theory that low PGM activity might be responsible for the partial inhibition of the glucose to lactate conversion, in retrospect PGM activity might only be one factor that contributed to this observation.

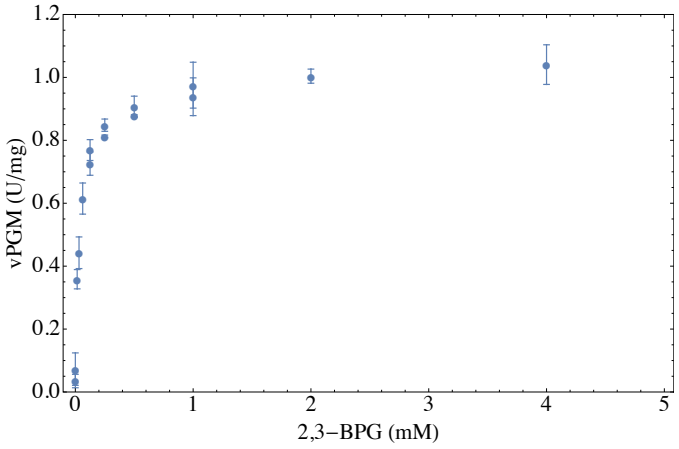

Figure A.1: 2,3-BPG induced activation of PGM. Conducted the enzyme assay at 10mM 3-PG. We only one biological repeat was measured (n = 1). The data points is shown as mean ± SD of the technical triplicate.

Bibliography

[1] Organization, W.H. *et al.*: Who report on cancer: setting priorities, investing wisely and providing care for all. 2020.

[2] DeBerardinis, R.J. and Chandel, N.S.: Fundamentals of cancer metabolism. *Science advances*, vol. 2, no. 5, p. e1600200, 2016.

[3] Vander Heiden, M.G. and DeBerardinis, R.J.: Understanding the intersections between metabolism and cancer biology. *Cell*, vol. 168, no. 4, pp. 657–669, 2017.

[4] Pavlova, N.N. and Thompson, C.B.: The emerging hallmarks of cancer metabolism. *Cell metabolism*, vol. 23, no. 1, pp. 27–47, 2016.

[5] Gill, K.S., Fernandes, P., O'Donovan, T.R., McKenna, S.L., Doddakula, K.K., Power, D.G., Soden, D.M. and Forde, P.F.: Glycolysis inhibition as a cancer treatment and its role in an anti-tumour immune response. *Biochimica et Biophysica Acta (BBA)-Reviews on Cancer*, vol. 1866, no. 1, pp. 87–105, 2016.

[6] Medina, M.Á.: Mathematical modeling of cancer metabolism. *Critical reviews in oncology/hematology*, vol. 124, pp. 37–40, 2018.

[7] Kitano, H.: Systems biology: a brief overview. *science*, vol. 295, no. 5560, pp. 1662–1664, 2002.

[8] Marín-Hernández, A., Gallardo-Pérez, J.C., Rodríguez-Enríquez, S., Encalada, R., Moreno-Sánchez, R. and Saavedra, E.: Modeling cancer glycolysis. *Biochimica et Biophysica Acta (BBA)-Bioenergetics*, vol. 1807, no. 6, pp. 755–767, 2011.

[9] Teusink, B., Passarge, J., Reijenga, C.A., Esgalhado, E., Van der Weijden, C.C., Schepper, M., Walsh, M.C., Bakker, B.M., Van Dam, K., Westerhoff, H.V. *et al.*: Can yeast glycolysis be understood in terms of in vitro kinetics of the constituent enzymes? testing biochemistry. *European Journal of Biochemistry*, vol. 267, no. 17, pp. 5313–5329, 2000.

[10] Shestov, A.A., Liu, X., Ser, Z., Cluntun, A.A., Hung, Y.P., Huang, L., Kim, D., Le, A., Yellen, G., Albeck, J.G. *et al.*: Quantitative determinants of aerobic glycolysis identify flux through the enzyme gapdh as a limiting step. *elife*, vol. 3, p. e03342, 2014.

[11] Fell, D. and Cornish-Bowden, A.: *Understanding the control of metabolism*, vol. 2. Portland press London, 1997.

[12] Tanner, L.B., Goglia, A.G., Wei, M.H., Sehgal, T., Parsons, L.R., Park, J.O., White, E., Toettcher, J.E. and Rabinowitz, J.D.: Four key steps control glycolytic flux in mammalian cells. *Cell systems*, vol. 7, no. 1, pp. 49–62, 2018.

[13] Foulkes, W.D., Smith, I.E. and Reis-Filho, J.S.: Triple-negative breast cancer. *New England journal of medicine*, vol. 363, no. 20, pp. 1938–1948, 2010.

[14] Lunetti, P., Di Giacomo, M., Vergara, D., De Domenico, S., Maffia, M., Zara, V., Capobianco, L. and Ferramosca, A.: Metabolic reprogramming in breast cancer results in distinct mitochondrial bioenergetics between luminal and basal subtypes. *The FEBS journal*, vol. 286, no. 4, pp. 688–709, 2019.

[15] Zordoky, B.N., Bark, D., Soltys, C.L., Sung, M.M. and Dyck, J.R.: The anti-proliferative effect of metformin in triple-negative mda-mb-231 breast cancer cells is highly dependent on glucose concentration: implications for cancer therapy and prevention. *Biochimica et Biophysica Acta (BBA)-General Subjects*, vol. 1840, no. 6, pp. 1943–1957, 2014.

[16] Li, N., Deng, Y., Zhou, L., Tian, T., Yang, S., Wu, Y., Zheng, Y., Zhai, Z., Hao, Q., Song, D. *et al.*: Global burden of breast cancer and attributable risk factors in 195 countries and territories, from 1990 to 2017: results from the global burden of disease study 2017. *Journal of Hematology & Oncology*, vol. 12, no. 1, p. 140, 2019.

[17] Hu, K., Ding, P., Wu, Y., Tian, W., Pan, T. and Zhang, S.: Global patterns and trends in the breast cancer incidence and mortality according to sociodemographic indices: an observational study based on the global burden of diseases. *BMJ open*, vol. 9, no. 10, p. e028461, 2019.

[18] Hanahan, D. and Weinberg, R.A.: Hallmarks of cancer: the next generation. *cell*, vol. 144, no. 5, pp. 646–674, 2011.

[19] Vander Heiden, M.G., Cantley, L.C. and Thompson, C.B.: Understanding the warburg effect: the metabolic requirements of cell proliferation. *science*, vol. 324, no. 5930, pp. 1029–1033, 2009.

[20] TeSlaa, T. and Teitell, M.A.: Techniques to monitor glycolysis. In: *Methods in enzymology*, vol. 542, pp. 91–114. Elsevier, 2014.

[21] Potter, M., Newport, E. and Morten, K.J.: The warburg effect: 80 years on. *Biochemical Society Transactions*, vol. 44, no. 5, pp. 1499–1505, 2016.

[22] Sciacovelli, M., Gaude, E., Hilvo, M. and Frezza, C.: The metabolic alterations of cancer cells. In: *Methods in enzymology*, vol. 542, pp. 1–23. Elsevier, 2014.

[23] Fadaka, A., Ajiboye, B., Ojo, O., Adewale, O., Olayide, I. and Emuowhochere, R.: Biology of glucose metabolization in cancer cells. *Journal of Oncological Sciences*, vol. 3, no. 2, pp. 45–51, 2017.

[24] Masui, K., Cavenee, W.K. and Mischel, P.S.: mtorc2 in the center of cancer metabolic reprogramming. *Trends in Endocrinology & Metabolism*, vol. 25, no. 7, pp. 364–373, 2014.

[25] Bardini, R., Politano, G., Benso, A. and Di Carlo, S.: Multi-level and hybrid modelling approaches for systems biology. *Computational and structural biotechnology journal*, vol. 15, pp. 396–402, 2017.

[26] Marzen, S., Garcia, H.G. and Phillips, R.: Statistical mechanics of monod–wyman–changeux (mwc) models. *Journal of molecular biology*, vol. 425, no. 9, pp. 1433–1460, 2013.

[27] Noor, E., Flamholz, A., Liebermeister, W., Bar-Even, A. and Milo, R.: A note on the kinetics of enzyme action: a decomposition that highlights thermodynamic effects. *FEBS letters*, vol. 587, no. 17, pp. 2772–2777, 2013.

[28] Moreno-Sánchez, R., Saavedra, E., Rodríguez-Enríquez, S. and Olín-Sandoval, V.: Metabolic control analysis: a tool for designing strategies to manipulate metabolic pathways. *BioMed Research International*, vol. 2008, 2008.

[29] Haanstra, J.R., Gerding, A., Dolga, A.M., Sorgdrager, F.J., Buist-Homan, M., Du Toit, F., Faber, K.N., Holzhütter, H.-G., Szöör, B., Matthews, K.R. *et al.*: Targeting pathogen metabolism without collateral damage to the host. *Scientific reports*, vol. 7, p. 40406, 2017.

[30] House, S.W., Warburg, O., Burk, D. and Schade, A.L.: On respiratory impairment in cancer cells. *Science*, vol. 124, no. 3215, pp. 267–272, 1956.

[31] Diaz-Ruiz, R., Uribe-Carvajal, S., Devin, A. and Rigoulet, M.: Tumor cell energy metabolism and its common features with yeast metabolism. *Biochimica et Biophysica Acta (BBA)-Reviews on Cancer*, vol. 1796, no. 2, pp. 252–265, 2009.

[32] Diaz-Ruiz, R., Rigoulet, M. and Devin, A.: The warburg and crabtree effects: On the origin of cancer cell energy metabolism and of yeast glucose repression. *Biochimica et Biophysica Acta (BBA)-Bioenergetics*, vol. 1807, no. 6, pp. 568–576, 2011.

[33] Hay, N.: Reprogramming glucose metabolism in cancer: can it be exploited for cancer therapy? *Nature Reviews Cancer*, vol. 16, no. 10, p. 635, 2016.

[34] Ngo, D.C., Ververis, K., Tortorella, S.M. and Karagiannis, T.C.: Introduction to the molecular basis of cancer metabolism and the warburg effect. *Molecular biology reports*, vol. 42, no. 4, pp. 819–823, 2015.

[35] Dumas, J.-F., Brisson, L., Chevalier, S., Mahéo, K., Fromont, G., Moussata, D., Besson, P. and Roger, S.: Metabolic reprogramming in cancer cells, consequences on ph and tumour progression: integrated therapeutic perspectives with dietary lipids as adjuvant to anticancer treatment. In: *Seminars in cancer biology*, vol. 43, pp. 90–110. Elsevier, 2017.

[36] Ždralević, M., Marchiq, I., de Padua, M.M.C., Parks, S.K. and Pouysségur, J.: Metabolic plasiticy in cancersâdistinct role of glycolytic enzymes gpi, ldhs or membrane transporters mcts. *Frontiers in oncology*, vol. 7, p. 313, 2017.

[37] Marin-Hernandez, A., Gallardo-Perez, J.C., Ralph, S.J., Rodriguez-Enriquez, S. and Moreno-Sanchez, R.: Hif-1α modulates energy metabolism in cancer cells by inducing over-expression of specific glycolytic isoforms. *Mini reviews in medicinal chemistry*, vol. 9, no. 9, pp. 1084–1101, 2009.

[38] Nowak, N., Kulma, A. and Gutowicz, J.: Up-regulation of key glycolysis proteins in cancer development. *Open Life Sciences*, vol. 13, no. 1, pp. 569–581, 2018.

[39] Warmoes, M.O. and Locasale, J.W.: Heterogeneity of glycolysis in cancers and therapeutic opportunities. *Biochemical pharmacology*, vol. 92, no. 1, pp. 12–21, 2014.

[40] Moreno-Sánchez, R., Marín-Hernández, A., Gallardo-Pérez, J.C., Quezada, H., Encalada, R., Rodríguez-Enríquez, S. and Saavedra, E.: Phosphofructokinase type 1 kinetics, isoform expression, and gene polymorphisms in cancer cells. *Journal of cellular biochemistry*, vol. 113, no. 5, pp. 1692–1703, 2012.

[41] Zancan, P., Sola-Penna, M., Furtado, C.M. and Da Silva, D.: Differential expression of phosphofructokinase-1 isoforms correlates with the glycolytic efficiency of breast cancer cells. *Molecular genetics and metabolism*, vol. 100, no. 4, pp. 372–378, 2010.

[42] Ros, S. and Schulze, A.: Balancing glycolytic flux: the role of 6-phosphofructo-2-kinase/fructose 2, 6-bisphosphatases in cancer metabolism. *Cancer & metabolism*, vol. 1, no. 1, p. 8, 2013.

[43] Dasgupta, S., Rajapakshe, K., Zhu, B., Nikolai, B.C., Yi, P., Putluri, N., Choi, J.M., Jung, S.Y., Coarfa, C., Westbrook, T.F. *et al.*: Metabolic enzyme pfkfb4 activates transcriptional coactivator src-3 to drive breast cancer. *Nature*, vol. 556, no. 7700, pp. 249–254, 2018.

[44] Zhang, D., Jin, N., Sun, W., Li, X., Liu, B., Xie, Z., Qu, J., Xu, J., Yang, X., Su, Y. *et al.*: Phosphoglycerate mutase 1 promotes cancer cell migration independent of its metabolic activity. *Oncogene*, vol. 36, no. 20, pp. 2900–2909, 2017.

[45] Christofk, H.R., Vander Heiden, M.G., Harris, M.H., Ramanathan, A., Gerszten, R.E., Wei, R., Fleming, M.D., Schreiber, S.L. and Cantley, L.C.: The m2 splice isoform of pyruvate kinase is important for cancer metabolism and tumour growth. *Nature*, vol. 452, no. 7184, pp. 230–233, 2008.

[46] Mazurek, S., Boschek, C.B., Hugo, F. and Eigenbrodt, E.: Pyruvate kinase type m2 and its role in tumor growth and spreading. In: *Seminars in cancer biology*, vol. 15, pp. 300–308. Elsevier, 2005.

[47] Chaneton, B., Hillmann, P., Zheng, L., Martin, A.C., Maddocks, O.D., Chokkathukalam, A., Coyle, J.E., Jankevics, A., Holding, F.P., Vousden, K.H. *et al.*: Serine is a natural ligand and allosteric activator of pyruvate kinase m2. *Nature*, vol. 491, no. 7424, pp. 458–462, 2012.

[48] Xie, J., Dai, C. and Hu, X.: Evidence that does not support pyruvate kinase m2 (pkm2)-catalyzed reaction as a rate-limiting step in cancer cell glycolysis. *Journal of Biological Chemistry*, vol. 291, no. 17, pp. 8987–8999, 2016.

[49] Moreno-Sánchez, R., Rodríguez-Enríquez, S., Marín-Hernández, A. and Saavedra, E.: Energy metabolism in tumor cells. *The FEBS journal*, vol. 274, no. 6, pp. 1393–1418, 2007.

[50] Gaglio, D., Metallo, C.M., Gameiro, P.A., Hiller, K., Danna, L.S., Balestrieri, C., Alberghina, L., Stephanopoulos, G. and Chiaradonna, F.: Oncogenic k-ras decouples glucose and glutamine metabolism to support cancer cell growth. *Molecular systems biology*, vol. 7, no. 1, 2011.

[51] Kim, J.-w. and Dang, C.V.: Multifaceted roles of glycolytic enzymes. *Trends in biochemical sciences*, vol. 30, no. 3, pp. 142–150, 2005.

[52] Gupta, C. and Tikoo, K.: High glucose and insulin differentially modulates proliferation in mcf-7 and mda-mb-231 cells. *J Mol Endocrinol*, vol. 51, no. 1, pp. 119–29, 2013.

[53] Ocaña, M., Martínez-Poveda, B., Quesada, A.R. and Medina, M.Á.: Glucose favors lipid anabolic metabolism in the invasive breast cancer cell line mda-mb-231. *Biology*, vol. 9, no. 1, p. 16, 2020.

[54] Wise, D.R., DeBerardinis, R.J., Mancuso, A., Sayed, N., Zhang, X.-Y., Pfeiffer, H.K., Nissim, I., Daikhin, E., Yudkoff, M., McMahon, S.B. *et al.*: Myc regulates a transcriptional program that stimulates mitochondrial glutaminolysis and leads to glutamine addiction. *Proceedings of the National Academy of Sciences*, vol. 105, no. 48, pp. 18782–18787, 2008.

[55] DeBerardinis, R.J., Mancuso, A., Daikhin, E., Nissim, I., Yudkoff, M., Wehrli, S. and Thompson, C.B.: Beyond aerobic glycolysis: transformed cells can engage in glutamine metabolism that exceeds the requirement for protein and nucleotide synthesis. *Proceedings of the National Academy of Sciences*, vol. 104, no. 49, pp. 19345–19350, 2007.

[56] Penkler, G., Du Toit, F., Adams, W., Rautenbach, M., Palm, D.C., Van Niekerk, D.D. and Snoep, J.L.: Construction and validation of a detailed kinetic model of glycolysis in plasmodium falciparum. *The FEBS journal*, vol. 282, no. 8, pp. 1481–1511, 2015.

[57] Marín-Hernández, A., López-Ramírez, S.Y., Del Mazo-Monsalvo, I., Gallardo-Pérez, J.C., Rodríguez-Enríquez, S., Moreno-Sánchez, R. and Saavedra, E.: Modeling cancer glycolysis under hypoglycemia, and the role played by the

differential expression of glycolytic isoforms. *The FEBS journal*, vol. 281, no. 15, pp. 3325–3345, 2014.

[58] Damiani, C., Colombo, R., Gaglio, D., Mastroianni, F., Pescini, D., Westerhoff, H.V., Mauri, G., Vanoni, M. and Alberghina, L.: A metabolic core model elucidates how enhanced utilization of glucose and glutamine, with enhanced glutamine-dependent lactate production, promotes cancer cell growth: The warburq effect. *PLoS computational biology*, vol. 13, no. 9, p. e1005758, 2017.

[59] Kelly, R.A., Leedale, J., Harrell, A., Beard, D.A., Randle, L.E., Chadwick, A.E. and Webb, S.D.: Modelling the impact of changes in the extracellular environment on the cytosolic free nad+/nadh ratio during cell culture. *PloS one*, vol. 13, no. 11, 2018.

[60] Liberti, M.V., Dai, Z., Wardell, S.E., Baccile, J.A., Liu, X., Gao, X., Baldi, R., Mehrmohamadi, M., Johnson, M.O., Madhukar, N.S. *et al.*: A predictive model for selective targeting of the warburg effect through gapdh inhibition with a natural product. *Cell metabolism*, vol. 26, no. 4, pp. 648–659, 2017.

[61] Marín-Hernández, A., Rodríguez-Enríquez, S., Vital-González, P.A., Flores-Rodríguez, F.L., Macías-Silva, M., Sosa-Garrocho, M. and Moreno-Sánchez, R.: Determining and understanding the control of glycolysis in fast-growth tumor cells: Flux control by an over-expressed but strongly product-inhibited hexokinase. *The FEBS journal*, vol. 273, no. 9, pp. 1975–1988, 2006.

[62] Bradford, M.M.: A rapid and sensitive method for the quantitation of microgram quantities of protein utilizing the principle of protein-dye binding. *Analytical biochemistry*, vol. 72, no. 1-2, pp. 248–254, 1976.

[63] Brodsky, A.N., Odenwelder, D.C. and Harcum, S.W.: High extracellular lactate causes reductive carboxylation in breast tissue cell lines grown under normoxic conditions. *PloS one*, vol. 14, no. 6, 2019.

[64] van Dyk, J.B.: Mathematical modelling of glycolysis in skeletal muscle cells.

Addendum

A.1 Supplementary table

Table 1: An overview of all parameters (V_{max} and K_m) that were sourced from the literature to construct the MDA-mb-231 model.

Maximal specific activities and affinity constants			
Enzyme	Parameter	Fitted Value	References
ALD	K_{GAP} (mM)	0.16	[8]
	K_{DHAP} (mM)	0.08	[8]
TPI	K_{DHAP} (mM)	1.6	[8]
	$V_{f\,GAPDH}$ (μmol.min^{-1}.mg^{-1} protein)	1.0 $\pm$ 0.038	[48]
GAPDH	K_{GAP} (mM)	0.19	[8]
	K_{NAD^+} (mM)	0.09	[8]
PGK	K_{B13PG} (mM)	0.079	[8]
	K_{ADP} (mM)	0.4	[8]
ENO	K_{PEP} (mM)	0.06	[8]
ATPase	$V_{f\,ATPase}$ (μmol.min^{-1}.mg^{-1} protein)	0.0021 $\pm$ 0.0002	[64]